

Influence of the cation distribution, atomic substitution, and atomic vacancies on the physical properties of $CoFe_2O_4$ and $NiFe_2O_4$ spinel ferrites

Kedar Sharma ¹, Lionel Calmels ¹, Dongzhe Li ¹, Antoine Barbier ² and Rémi Arras ^{1,*}

¹*CEMES, Université de Toulouse, CNRS, 29 rue Jeanne Marvig, F-31055 Toulouse, France*

²*Service de Physique de l'Etat Condensé, CEA, CNRS UMR 3680, Université Paris-Saclay, CEA Saclay, 91191 Gif-sur-Yvette Cedex, France*

 (Received 16 May 2022; revised 22 September 2022; accepted 14 November 2022; published 5 December 2022)

$CoFe_2O_4$ and $NiFe_2O_4$ are well-known insulating and ferrimagnetic spinel ferrites with high Curie temperatures, an important characteristic for electronic and spintronic applications. We used first-principles calculations to investigate how their electronic and magnetic properties can be altered or tuned by the presence of structural point defects. We considered successively the effects of cation distribution in the spinel lattice for stoichiometric compounds and of atom substitutions or vacancies. Our calculations demonstrate that a deviation from the perfectly inverse distribution of cations increases the magnetization and decreases the width of the band gap at the Fermi level. In contrast to cation vacancies, oxygen vacancies are not expected to strongly affect the magnetization. We show that $NiFe_2O_4$ crystals with an excess of Ni cations can display a spin-polarized hole conductivity. We finally calculated the formation energy of the different defects and we give details on their gap states.

DOI: [10.1103/PhysRevMaterials.6.124402](https://doi.org/10.1103/PhysRevMaterials.6.124402)

I. INTRODUCTION

Transition-metal oxides form a large family of materials that have attracted a lot of interest for several years, due to their various and highly-tunable physical properties. These compounds are now widely recognized as fruitful playgrounds for fundamental studies as well as serious candidates for many applications [1]. Among this family of materials, spinel ferrites MFe_2O_4 (M being a transition-metal atom) particularly deserve attention. They have already been considered for applications in many scientific and technical fields, ranging from medicine [2–5], chemistry and catalysis [6,7], energy [8] and water splitting [9], to electronics and spintronics [10,11]. Partly formed by some of the most abundant chemical species on earth, they possess a complex atomic structure and mixed and tunable valency states. While they are parent compounds of magnetite Fe_3O_4 , a material, which has been theoretically predicted half-metallic at room temperature in its bulk form [12], many MFe_2O_4 spinel ferrites, such as $CoFe_2O_4$ (CFO) or $NiFe_2O_4$ (NFO), are insulating. These compounds have moreover in common to be ferrimagnetic with a Curie temperature T_C well above room temperature (793 K for CFO and 850 K for NFO), which makes them particularly interesting for spintronic applications [10,11], like magnetic tunnel barriers for spin-polarized tunneling [13], magnetoelectric multiferroic heterostructures [14–16], magneto-ionic systems or magnetic resistive random access memories (ReRAM) [17–21].

Spinel ferrites adopt the same atomic structure as $MgAl_2O_4$, with a distorted face-centred cubic lattice of oxygen atoms, which displays tetrahedral (Td) and octahedral

(Oh) atomic sites; one eighth of the Td sites and half of the octahedral sites are occupied by the M and Fe cations, the details of this distribution depending on the chemical nature of the cation M [22]. In the case of CFO and NFO, $M = Co$ or Ni will be divalent cations, while Fe cations will ideally be present in the +III oxidation state. Both CFO and NFO are known to mainly adopt the inverse spinel structure, which means that the $Co(II)$ or $Ni(II)$ cations are sharing the occupied Oh sites with half of the $Fe(III)$ cations, while the other half of the $Fe(III)$ are located in Td atomic sites. Deviations from this perfect cation distribution is depicted by the inversion parameter λ ($0 \leq \lambda \leq 1$). The chemical formula describing the structure of the partially inverted spinel ferrite MFe_2O_4 can be written as $(M_{1-\lambda}^{2+}Fe_{\lambda}^{3+})_{Td}[M_{\lambda}^{2+}Fe_{2-\lambda}^{3+}]_{Oh}O_4^{2-}$, $\lambda = 1$ corresponding to the perfect inverse spinel structure.

A complete description and understanding of the bulk properties of these spinel ferrites is essential to confirm their ability to be used in spintronic devices. Two main structural effects may modify the physical properties of spinel ferrites. On the one hand, the (+II, +III) cation distribution inside the occupied octahedral site sublattice (for the perfectly inverse structure) or between occupied tetrahedral and octahedral sites (for the partially inverted structure) is crucial, as it may affect electronic, magnetic, and optical properties [23]. On the other hand, deviations from the perfect MFe_2O_4 stoichiometry also modify the physical properties of the spinel ferrites: One of the main effects expected from atom vacancies will be to induce a charge reorganization, with local modifications of the valence charge states and the possible creation of defect gap states, which will change the magnetization and the electronic, ionic, or tunnel conductivities [18,24–28].

The presence of these two kinds of structural defects in a sample will depend on the nature of the cation M , the

*remi.arras@cemes.fr

dimensionality (nanoparticle, wire, film, or bulk) and size of the sample and of course, on the growth method and growth conditions. Even if information on the actual atomic structure of a sample can sometimes be inferred by measuring its magnetic or transport properties, a clear understanding of the link between these physical properties and the atomic structure of the sample often requires to use either spectroscopic techniques such as x-ray absorption, electron-energy loss, neutron, Mössbauer, or Raman spectroscopies [23], or calculations of the physical properties of the materials from methods based on first principles.

In this paper, we intend to enrich the already-available literature on CFO and NFO bulk crystals [18,28–33] with a number of not yet well-established aspects: We describe in detail the calculated electronic and magnetic properties of CFO and NFO, focusing on the effects of cation ordering in Oh and Td sites and on possible deviations from the perfect stoichiometry. We also include a detailed thermodynamic analysis of the stability of these oxides and a study of the different charged or neutral atom vacancies.

II. DETAILS ON THE CALCULATION METHODS

We performed first-principles calculations based on the density-functional theory (DFT). We used the *ab initio* code VASP [34,35] and the projector augmented wave (PAW) method [36], with the potentials generated for Fe($3s^23p^63d^74s^1$), Co($3s^23p^63d^84s^1$), Ni($3p^63d^94s^1$), and O($2s^22p^6$) configurations for valence electrons. We used a cutoff energy for the plane-wave-basis set of 600 eV. The exchange-correlation functional was expressed within the generalized-gradient approximation parametrized by Perdew, Burke, and Ernzerhof and revised for solids (GGA-PBESol) [37]. A Hubbard correction was added to take the strong correlations of the transition metal $3d$ bands into account. This has been done within the framework of the *DFT + U* formalism [38] and for the parameter $U_{\text{eff}} = (U - J)$ we used the values of 4.0 eV for Fe and Co atoms and of 2.5 eV for Ni atoms. These values have been chosen to obtain a good compromise between calculated band gaps and lattice parameters, by comparing our results calculated for perfect spinel crystals with experimental data found in the literature. Our chosen U_{eff} values are close from other values generally used in the literature [6,29,30,32,39–41].

To calculate the effects of atom vacancies, we used a supercell approach with a $1 \times 1 \times 1$ conventional cubic cell of 8 formula units (f.u.), i.e., 56 atoms. A Monkhorst-Pack grid [42] of $6 \times 6 \times 6$ \mathbf{k} vectors was used to sample the first Brillouin zone. Atomic positions and lattice parameters were optimized by minimizing the forces down to 10^{-4} eV/Å.

When studying the cation distribution in Sec. III A, we calculated the ground-state energy of the most stable structures with different collinear magnetic ordering. The standard ferrimagnetic ordering, consisting in an antiferromagnetic coupling between cations in tetrahedral and octahedral sites, was always found the most stable (see Sec. III A in the Supplemental Material [43]). This magnetic ordering was kept for the study of nonstoichiometric structures. Calculations with noncollinear magnetism have also been performed for a limited number of structures. In that case, we started from the

structure already optimized with the collinear ferrimagnetic ordering. A self-consistent calculation was then done including the spin-orbit interaction and allowing a noncollinear ordering to emerge, starting from the ferrimagnetic ordering and keeping the atomic structure and symmetries fixed.

To study the effects of the cation distribution, we first compared the total energies of the most ordered structures generated from the same conventional cell. We thus identified the most stable cation arrangements and, for the sake of simplicity, we used their primitive cells (which were found to contain 4 f.u. of $M\text{Fe}_2\text{O}_4$) to calculate the effects of cation swaps, of which the number was chosen as a parameter to quantify the cation disorder. Space groups have been determined using the FINDSYM software [44] and they are numbered and labeled according to the Bilbao Crystallographic Server [45,46]. The Site Occupancy Disorder (SOD) code has been used to generate the crystallographic configurations obtained with different cation orderings in Oh atomic sites [47].

Formation energies $E_f[V_X^q]$ of single X-atom vacancies V_X with charge state q (discussed in Sec. III B) have been calculated according to the following formula from Refs. [48–50],

$$E_f[V_X^q] = E[\text{Host} + V_X^q] - E[\text{Host}] + \mu_X + q(E_{\text{VBM}}^H + \Delta E_F) + E_{\text{corr}} \quad (1)$$

where $E[\text{Host} + V_X^q]$ and $E[\text{Host}]$ are the total energies calculated by DFT methods, respectively for the defective and nondefective cubic cells. μ_X is the chemical potential of the atom removed to form the vacancy. For each of the studied compounds, μ_X deviates by $\Delta\mu_X$ from the energy E_X^{elem} of the same chemical species in its pure solid or gas form, $\mu_X = E_X^{\text{elem}} + \Delta\mu_X$. The values of $\Delta\mu_X$ are calculated by considering the relative stability of the studied compound compared to other competitive materials (for more details, see Appendix). In the following, we will discuss the formation energies of atom vacancies calculated in the case of oxygen-rich ($\Delta\mu_O = -0.5$ eV) or oxygen-poor ($\Delta\mu_O = -2.2$ eV) experimental growth conditions as explained in the Appendix. Equation (1) can easily be extended to calculate the formation energy of a bivacancy.

The term $q(E_{\text{VBM}}^H + \Delta E_F)$, also equal to qE_F , corresponds to the chemical potential of the added or removed electrons, i.e., the modification of the energy due to the charge state of the defect; this quantity depends on the value of the Fermi level E_F within the fundamental band gap E_g of the material [here defined as the energy difference between the conduction band minimum (CBM) and the valence band maximum (VBM), independently of the spin state]. The Fermi energy E_F is the sum of E_{VBM}^H , the energy of the VBM for the bulk host crystal, and ΔE_F , the variation of the Fermi level in the gap with respect to the VBM.

Finally, E_{corr} is the Lany-Zunger correction [51], which includes the Makov-Payne correction [52] and a potential alignment, to correct for the shift of the electrostatic potential due to the limited size of the supercell. This correction is calculated using the PyDEF2 code [49,53]; it depends on the values of the relative permittivity that we calculated, 14.59 for NFO and 15.58 for CFO, in agreement for the latter with previously calculated (16.05) and measured ($\simeq 14$) values [54].

From the term $q(E_{\text{VBM}}^{\text{H}} + \Delta E_{\text{F}})$, we can infer that specific vacancies with a given charge state q will be more or less stable depending on the position of the Fermi level ΔE_{F} in the band gap of the spinel ferrite. The transition energies $\varepsilon(q_1/q_2)$ between two charge states q_1 and q_2 can be expressed as [48]

$$\varepsilon(q_1/q_2) = \frac{E_{\text{f}}[V_{\text{X}}^{q_1}, \Delta E_{\text{F}} = 0] - E_{\text{f}}[V_{\text{X}}^{q_2}, \Delta E_{\text{F}} = 0]}{q_2 - q_1}. \quad (2)$$

The energy of each charged structure has been calculated after optimization of the lattice parameters and atom coordinates, so each charged-state transition energy $\varepsilon(q_1/q_2)$ also takes into account the contribution of the lattice relaxation.

An equilibrium Fermi level can be calculated for specific growth conditions. It depends on the temperature T and on the concentration of X-atom vacancies with charge state q through the following electrical-neutrality equation [55,56]:

$$p - n + \sum_{\text{X},q} q[V_{\text{X}}^q] = 0 \quad (3)$$

where n and p are respectively the temperature-dependent concentrations of electrons at the bottom of the conduction band and holes at the top of the valence band for the bulk oxide $M\text{Fe}_2\text{O}_4$,

$$n = N_{\text{c}}(T) \exp\left[\frac{E_{\text{F}} - E_{\text{CBM}}}{k_{\text{B}}T}\right] \quad (4)$$

and

$$p = N_{\text{v}}(T) \exp\left[\frac{E_{\text{VBM}} - E_{\text{F}}}{k_{\text{B}}T}\right]. \quad (5)$$

$N_{\text{c(v)}}(T) = \left(\frac{2\pi m_{\text{c(h)}}^* k_{\text{B}}T}{h^2}\right)^{3/2}$ are the effective carrier densities of states near the bottom of the conduction (c) band and top of the valence (v) band, which depend on the effective mass of the electrons [$m_{\text{e}}^*(\text{CFO}) = 1.68 m_0$, $m_{\text{e}}^*(\text{NFO}) = 8.91 m_0$] and holes [$m_{\text{h}}^*(\text{CFO}) = 2.99 m_0$, $m_{\text{h}}^*(\text{NFO}) = 1.46 m_0$], where m_0 is the free electron mass. These formula are derived from the parabolic band approximation and in our calculations we only considered a single and nondegenerate band for the CBM and VBM.

The concentration of the atom vacancies $[V_{\text{X}}^q]$ depends on the formation energy of this defect, on the concentration $[X]$ of the X atoms in the bulk compound $M\text{Fe}_2\text{O}_4$ and on the temperature T ,

$$[V_{\text{X}}^q] = [X] \exp\left[-\frac{E_{\text{f}}(V_{\text{X}}^q)}{k_{\text{B}}T}\right] \quad (6)$$

with k_{B} the Boltzmann constant.

Because the formation energies $E_{\text{f}}(V_{\text{X}}^q)$ are function of the Fermi level, the equilibrium Fermi level must be determined self-consistently. We chose to calculate the Fermi level in the framework of the ‘‘defect freezing-in’’ [57]: First, the concentration of each vacancy is calculated according to Eqs. (3)–(6) at a high temperature $T_{\text{g}} = 673$ K, which is close to some reported growth temperatures [58,59]; then, considering that the materials are quenched and that the Fermi level is further measured at room temperature, we calculate a new value for the Fermi level at $T_{\text{R}} = 298$ K, with the constrain that the concentration of defects for a given chemical species must

stay constant,

$$\sum_q [V_{\text{X}}^q(T_{\text{g}})] = \sum_q [V_{\text{X}}^q(T_{\text{R}})]. \quad (7)$$

More details on the intermediate data needed to obtain the results discussed throughout this paper, as well as some optimized NiFe_2O_4 structures, are provided in the Supplemental Material [43].

III. RESULTS

A. Physical properties of stoichiometric CFO and NFO crystals

Before studying the modifications of the physical properties induced by atom vacancies in the spinel ferrites, we first discuss the different properties of the stoichiometric $M\text{Fe}_2\text{O}_4$ ($M = \text{Co}, \text{Ni}$) bulk crystals. These data will further be used as references. Meanwhile, we propose to give new insight on the well-known problem of cation ordering.

Controlling and understanding the cation ordering in oxides is important, as it may help to improve or to obtain new physical properties [60–62]. $M\text{Fe}_2\text{O}_4$ are mixed-valence complex oxides combining divalent M and trivalent Fe cations and the question of cation ordering in these compounds is not new [22,63–68]. In the most simple scenario where CFO and NFO adopt a perfectly inverse spinel structure, the distribution of cations can be rather complicated due to the more or less disordered distribution in the occupied Oh atomic sites. Most of the studies addressing the problem of cation ordering in Oh sites focused on the thermodynamic stability and only little information can be found regarding its impact on the electronic and magnetic properties. In addition, most of the spinel ferrite samples, in particular those of CFO, present a partially-inverse structure, with exchanges of M - and Fe-cations between occupied Td and Oh sites. In this case, the inversion degree λ appears as an important parameter to explain the strong modifications of the magnetic and electronic properties [23], with a predicted increase of the band gap by ~ 1 eV [30] and of the total spin magnetic moment by $4 \mu_{\text{B}}/\text{f.u.}$ and $6 \mu_{\text{B}}/\text{f.u.}$, respectively when CFO or NFO switch from a perfectly inverse to a perfectly normal spinel structure; Raman spectroscopy has been used to show that these variations could linearly depend on λ [69].

1. Influence of the cation distribution in the occupied Oh sites of inverse spinel structures

When a spinel ferrite adopts the normal structure, all the $M(\text{II})$ cations are located in the occupied Td atomic sites and the space group is $227-Fd\bar{3}m$. The inverse spinel structure would preserve this space group, as long as the +II and +III cations are randomly distributed inside the occupied Oh sites. Depending on the chemical species M , cation ordering may also occur in the occupied Oh sites [70,71], which breaks symmetries and reduces the space group to a subgroup of $Fd\bar{3}m$. Using a supercell to perform DFT calculations also implies that one has to choose a specific cation distribution, more or less ordered depending on the size of the supercell: This choice may affect some of the results the more sensitive to symmetries.

a. Atomic structure. In the conventional cubic cell containing 8 $M\text{Fe}_2\text{O}_4$ f.u. (i.e., 56 atoms), 8 Fe(III) and 8 M (II) cations must be distributed among the 16 occupied Oh sites, leading to $\binom{16}{8} = 12870$ possible distributions. The number of nonequivalent structures can be reduced to 97, spread into 17 different space groups. While space groups with several symmetry operations are only associated with a small number of equivalent structures (only 6 equivalent structures for the space group 91- $P4_122$, for instance), low-symmetry space groups conversely possess a large number of nonequivalent possible structures (the space group 1- P_1 corresponds to 9312 different structures, among which 49 are nonequivalent); for the sake of simplicity, we have first randomly chosen one of the possible structures to study the 17 space groups.

As suggested in the literature and detailed below, we found out that the structures with the most homogeneous cation distributions are the most stable: Among all the studied structures, we found that the ground-state distribution corresponds to the space group 13- $P2/c$ for CFO and 91- $P4_122$ for NFO. The energy difference $\Delta E_{91,13} = E_{91} - E_{13}$ between these two stable phases is of 15 meV/f.u. for CFO and of -9 meV/f.u. for NFO (see Fig. 1).

The cation distribution of three of the most stable structures (space groups 13, 74, and 91) and of the least stable one (space group 115) are shown in Fig. 1 in the Supplemental Material [43]. The three stable structures share the characteristics to have an homogeneous distribution of first-neighbor cations, the occupied octahedra sites forming tetrahedra with two M^{2+} and two Fe^{3+} cations at their vertices. These three structures are thus fulfilling the Anderson conditions based on the predominance of short-range ordering [66]. For both CFO and NFO, the space group 115- $P4m2$, which consists in a superlattice with a perfect segregation of M and Fe atoms on each side of the cubic cell, is the least stable, with an energy of approximately 130 meV/f.u. above that of the most stable structure.

To our knowledge, the centrosymmetric space group 13- $P2/c$, found as the most stable for CFO, has never been studied or reported up to now in the literature. Interestingly, this space group only becomes the most stable when applying the $+U$ correction, the space group 91- $P4_122$ being more stable otherwise. The stability of the supercell with the space group 13- $P2/c$ could be a consequence of the electron correlations in CFO and may only be observed at low temperature and under very specific experimental conditions, in the same way that low symmetry space groups have been evidenced to explain the low-temperature charge ordering in magnetite [72]. An experimental determination of the actual lowest energy phase of CFO should not be easy to perform, as the CFO crystal probably shows local fluctuations of its cation distribution that may strongly depend on the growth conditions.

The structure corresponding to the space group 91- $P4_122$ is the most stable for NFO. It corresponds to the maximally homogeneous distribution of divalent and trivalent cations over the octahedral sites, thus representing the global minimum of the electrostatic energy. According to the point-ion electrostatic (PIE) model [73], this structure has been claimed to correspond to the universal space group for ordered inverse spinels at low temperature; this has been confirmed

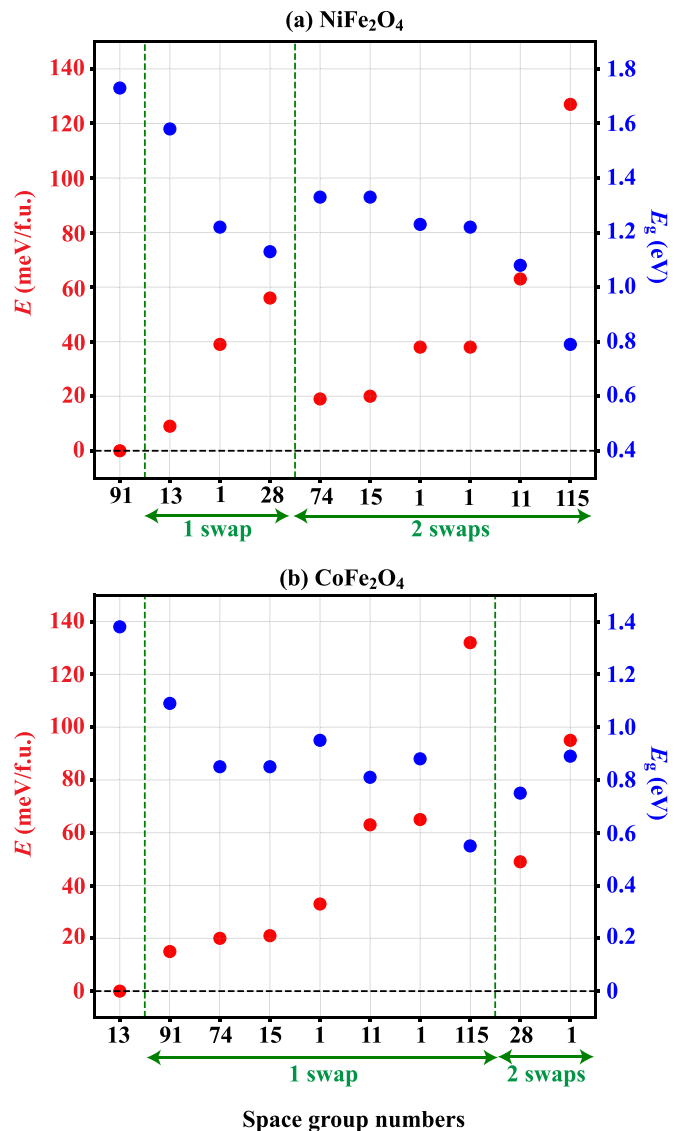


FIG. 1. Total energy E of the cubic conventional cell containing 8 f.u. of the perfect inverse spinels NiFe_2O_4 and CoFe_2O_4 and band-gap width E_g at the Fermi level E_F , as a function of the space group number [45,46]. The different space groups correspond to different cation distributions in the occupied Oh sites, which are generated by swapping one or two pair(s) of M/Fe atoms. The ground-state energy of the most stable structure is chosen as the origin of the energies and the space groups are ordered by increasing values of E . The band gap width E_g corresponds to the lowest energy difference between the highest occupied band and the lowest unoccupied band for one of the two spin directions.

experimentally on various compounds [74]. Our results for NFO are in agreement with former DFT studies [30,32,75], which however only compared a very small number of well-ordered inverse spinel structures. The predicted lowest energy space group of NFO also corresponds to that measured at 300 K on single crystals with Raman spectroscopy [70] or with synchrotron diffraction [71]. The authors of this last reference evidenced the emergence of an electric polarization associated with the cation ordering and the noncentrosymmetry

of the structure below 98 K, thus making this compound an intrinsic magnetoelectric multiferroic material [71,76].

In addition to the $91-P4_122$ space group (sometimes called α phase), the orthorhombic space group $74-Imma$ (β phase) is also often mentioned in the literature, as it corresponds to another short-range cation ordering for an inverse spinel structure [68,70]. The corresponding cation distribution presents an alternation of (001) Oh atomic layers with only $M(II)$ or $Fe(III)$ cations, while (100) and (010) layers present equal amounts of M and Fe atoms. For both CFO and NFO, the $Imma$ structure is found $\simeq 0.02$ eV/f.u. less stable than the lowest energy structure.

In the next sections of this paper, because the energy difference between the crystal cells with the $13-P2/c$ and $91-P4_122$ space groups is very small and for easier comparisons between NFO and CFO, we will mostly give details for the $P4_122$ space group, which will be considered as a bulk reference.

The calculated equilibrium pseudo-cubic lattice parameter $\langle a_0 \rangle = V^{1/3}$ (V being the volume of the conventional cubic cell) of the $P4_122$ reference structure is of 8.331 Å and 8.283 Å, respectively for CFO and NFO, which is 0.7% lower than the experimental values [77,78]. The calculated pseudo-cubic lattice parameter is the same (within 0.02%) for the four most stable structures of NFO. The tetragonal distortion inherent to the $P4_122$ space group is rather small ($c/a = 0.995$ for CFO and 1.002 for NFO).

b. Magnetic properties. For the cation distribution corresponding to the space group $P4_122$, we checked that the ferrimagnetic ordering is preserved in NFO and CFO and gives a lower energy than any of the other magnetic ordering, which have been tested [43]. Cations display parallel magnetic moments in each of the Td and Oh sublattices, which is imposed by the dominant antiferromagnetic coupling between cations belonging to the different sublattices. Such interactions were found constant on average for the most stable atomic structures [43]. The total spin magnetic moment $M_{f.u.}$ of the formula unit can thus be estimated by calculating the difference between the sum of the magnetic moments, in absolute value, of all the cations in Oh sites and of all those in Td sites. It can then be simplified as

$$M_{f.u.}(MFe_2O_4) = M(M_{Oh}^{2+}). \quad (8)$$

These equations are based on the hypothesis that all the cations in the CFO and NFO crystals with inverse spinel structure are perfectly ionized and described by the same electronic structures as if they were isolated ($3d^54s^0$, $3d^74s^0$, and $3d^84s^0$ for Fe^{3+} , Co^{2+} , and Ni^{2+} , respectively). The total spin magnetic moments stay exactly the same for all the inverse structures (i.e., independently of the cation distribution in Oh sites), with values of $M_{f.u.}(CFO) = 3 \mu_B$ and $M_{f.u.}(NFO) = 2 \mu_B$.

As we will show later, the analysis of the density-of-states (DOS) curves show that Ni^{2+} cations are in a low-spin state, while Co^{2+} cations are in a high-spin state. The nature of the spin state of the Ni^{2+} cations does not affect their spin magnetic moment, when they have a +2 oxidation state, i.e., in a perfect structure; the situation may be different near structural defects, due to charge transfers. For CFO, the energy difference calculated between configurations where Co^{2+} cations are in the low- and high-spin state is 0.63 eV/f.u. and the

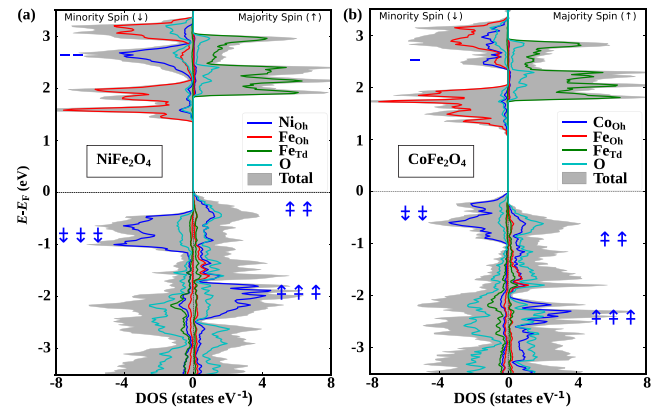


FIG. 2. Spin- and site-projected DOS (per formula unit) calculated for the perfect bulk (a) $NiFe_2O_4$ and (b) $CoFe_2O_4$ inverse spinel structures with the space group $P4_122$. Majority and minority spin DOS curves are respectively shown in the right and left panels of each subfigure. Blue lines next to the DOS, with/without arrows, show the theoretical orbital filling of Co^{2+} and Ni^{2+} cations.

total spin magnetic moment would decrease from $3 \mu_B$ /f.u. to $1 \mu_B$ /f.u. by transiting between these two states.

For the most stable structures, we also performed calculations including the spin-orbit interaction self-consistently. We found for CFO, that the magnetization easy axis is along the [001] direction for both the cation distributions of space groups $13-P/2c$ and $91-P4_122$, with a magnetocrystalline anisotropy energy between the [001] direction and the [110] direction of $\Delta E_{MCA} = E_{001} - E_{110} = -7.4 \mu eV \text{ \AA}^{-3}$ and $-33.6 \mu eV \text{ \AA}^{-3}$, respectively. For NFO (space group 91), the easy axis is on the contrary along the [110] direction, with $\Delta E_{MCA} = 0.9 \mu eV \text{ \AA}^{-3}$, that is one or two orders of magnitude lower than for CFO. A more detailed study of the changes of magnetic anisotropy as a function of the cation distribution can be found in Ref. [31].

For the cation distribution corresponding to the space-group 91, the spin magnetic moments of Co cations were found to display a small canting of 2.64° toward {110} directions, and are ordered such that the projection of the spin magnetic moment in the (001) planes is 0. A small canting of the Fe_{Td} atoms of 1.57° is also calculated along {100} directions. The total spin magnetic moment is decreased from $3 \mu_B$ for the collinear ordering to $2.989 \mu_B$ due to these spin cantings, i.e., by only 0.4%. The magnitude of the orbital magnetic moments of Co^{2+} cations is 12.5% that of their spin magnetic moments, while the orbital magnetic moment of Fe cations is almost null. Consequently, the orbital contribution to the total magnetic moment is only 9.5% (7.9% for the space group 13). No particular magnetic moment cantings are noticed in the case of NFO for which the orbital contribution to the total magnetic moment is 6.7%. Due to their low values and the computational cost for their computation, orbital magnetic moments will not be systematically discussed in the following.

c. Electronic structure. DOS curves are shown in Figs. 2(a) and 2(b), respectively for CFO and NFO. The fundamental Kohn-Sham band gap is delimited by the highest occupied band energy and the energy of the lowest unoccupied

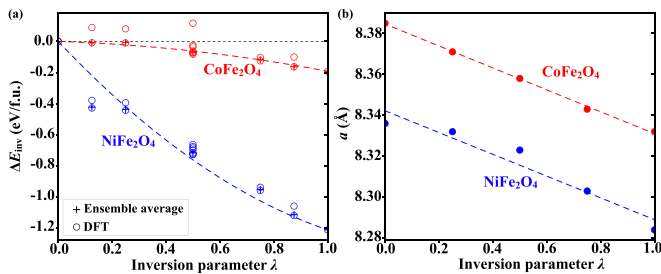


FIG. 3. (a) Variations of the total energy ΔE_{inv} and (b) of the pseudocubic lattice parameter a , as a function of the inversion parameter λ . ΔE_{inv} is given with respect to the energy of the perfect normal spinel structure, $\Delta E_{\text{inv}}(\lambda) = E(\lambda) - E(0)$. Open circles correspond to the energies calculated by DFT for all possible structures generated from the primitive cell with space group $P4_122$ ($\lambda = 0, 0.25, 0.5, 0.75, 1$) or from the conventional cell ($\lambda = 0.125, 0.875$). Crosses are the ensemble average of these calculated energies, which are used for the quadratic fits represented by the dashed lines. Lattice parameters are given for the most stable structures.

state, independently of the spin direction. For CFO, this band gap is located between the minority-spin VBM, where cobalt cations have a major contribution and by the minority spin CBM, which corresponds to Fe(Oh) bands. The CBM of NFO also corresponds to minority-spin unoccupied Fe(Oh), but its VBM corresponds to majority spin bands and to hybridization of Ni(Oh)- d and O- p orbitals, in agreement with Refs. [29,30,79]. The difference of spin polarization of the VBM between CFO and NFO comes from the fact that Co^{2+} cations adopt a high-spin state, while Ni^{2+} cations display a low-spin state; in consequences, the highest-occupied d bands will correspond to minority-spin t_{2g} -like orbitals for CFO and to majority-spin e_g -like orbitals for NFO (see the energy diagram in Fig. 3 in the Supplemental Material [43]). The fundamental band-gap energy E_g calculated for the $P4_122$ space group is of 1.09 eV for CFO and 1.34 eV for NFO.

Experimentally, optical band gaps have been measured in the energy ranges of 1.17–1.3 eV for CFO [28,41] and 1.52–1.65 eV for NFO [28,40,80]. Optical band-gap widths are associated with electronic transitions, which preserve the spin state and should thus be larger than the calculated fundamental band gaps. A direct comparison with our numerical calculations would necessitate to know precisely which electronic transitions they refer to. For a fixed spin direction, the lowest band gap is delimited by the highest occupied band and lowest unoccupied band of the minority spin channel, for both CFO and NFO. The values of these band gaps are given in Fig. 1. For the space group $P4_122$, they are respectively of 1.09 eV for CFO (equal to the fundamental band gap) and 1.73 eV for NFO, which is close to the experimental measurements. A comparison between our calculated values and other theoretical band gaps reported in the literature is difficult, owing to their large spread, from 0.63 to 1.5 eV for CFO [28–30,32,39,41,79,81,82] and from 0.98 to 2.27 eV for NFO [28,30,39,76,79–81,83]. Such a dispersion reflects the diversity of the numerical methods and approximations used to calculate the exchange–correlation potential for these compounds, which includes all the user-dependent corrections

(+ U , hybrid or meta-GGA), in principles needed to correctly reproduce the insulating behavior of CFO and NFO [84].

Starting from the most stable cation configuration and using the 4-f.u. primitive cell, we generated new structures by swapping 1 or 2 M/Fe atomic pairs located in occupied Oh sites. Fig. 1 displays the evolution of the ground-state energy and band gap width at the Fermi level as a function of the number of swaps. The variations of the calculated band gap width E_g as a function of the total energy for the different cation distributions are more random for CFO than for NFO. For both materials, however, the general trend is that of a decrease of E_g for the less stable structures. Hence, the calculated values of the fundamental band gap vary from 0.55 to 1.38 eV and from 0.57 to 1.34 eV, respectively for CFO and NFO. The few structures with an energy less than 0.03 eV/f.u. higher than that of the most stable one show band-gap variations of less than 25% for NFO and 38% for CFO, which suggests that the band-gap is more sensitive to cation disorder for CFO.

2. Influence of the inversion degree on the physical properties

Measurable experimentally, the deviations of the M/Fe cation distribution between Td and Oh atomic sites away from that of the perfect inverse spinel must be considered, as they do modify the physical and chemical properties of spinel ferrites, such as the magnetization or the lattice parameter. Before being studied by DFT-based methods [29,30,79], the influence of the inversion degree parameter λ on the physical properties of spinel oxides had first been investigated by phenomenological models based on the concepts of crystal-field stabilization energy (CFSE) and of octahedra site preference energy (OSPE), which consists in the difference of CFSE between octahedra and tetrahedra sites. The cation location depends on the number of coordination, on the number of electrons occupying their d orbitals (cations with a higher charge preferentially occupying Oh sites, because they offer a higher coordination degree) and on the orbital radii, which depend on the cation electronegativity [22] (smaller atoms being preferentially located in Td atomic sites). M and Fe cations with a high atomic radius will be responsible for a distortion of the oxygen atom sublattice, which allows accommodating the presence of these chemical species in their crystallographic sites. The crystal-field theory can however be insufficient and must be improved by adding the Madelung energy [65,67] or by including temperature effects through Monte Carlo simulations [73,85]; such a method allowed Stevanović, *et al.* to determine the inversion character of a spinel crystal as a function of the charges of the two cations and of the structural distortion u of the oxygen sublattice [85].

a. Atomic structure. As written in the introduction, the cation distribution in a crystal with a not-perfectly-inverse spinel structure can be described by the formula $(M_{1-\lambda}^{2+}Fe_{\lambda}^{3+})_{\text{Td}}[M_{\lambda}^{2+}Fe_{2-\lambda}^{3+}]_{\text{Oh}}O_4^{2-}$, $\lambda = 0(1)$ corresponding to a normal(inverse) spinel structure. Figure 3(a) shows the variations ΔE_{inv} of the total energy of the supercell when λ decreases from 1 to 0. Several structures corresponding to different cation distributions for a given value of λ have been calculated (see more details in the Supplemental Material [43]); their energy differences spread at most in

a range of 0.065 eV/f.u. and 0.198 eV/f.u. for NFO and CFO respectively, CFO showing larger spreading than NFO. The λ dependence of the ensemble-averaged value ΔE_{inv} is quadratic [86] and our calculated energy difference between the normal and inverse cation distribution $\Delta E_{\text{inv}}(\lambda = 1) = E(\lambda = 1) - E(\lambda = 0)$ is of approximately -1.21 eV/f.u. for NiFe_2O_4 and -0.19 eV/f.u. for CFO, i.e., almost six times lower, which confirms that NFO is more susceptible to be found with a perfectly inverse spinel structure. A qualitative agreement is found between our data and previously-reported results, with $\Delta E_{\text{inv}}(\lambda = 1)$ varying from -0.34 to -0.19 eV/f.u. for CFO [29,30,82] and calculated to -0.89 eV/f.u. for NFO [30].

Using the variations of $\Delta E_{\text{inv}}(\lambda)$, we calculated the configurational Gibbs free energy, which allows us to determine the equilibrium inversion parameter of each oxide as a function of the growth temperature T_g [87,88] (see Sec. II B in the Supplemental Material [43]). For $T_g = 600$ K, we found that an equilibrium λ of 0.955 and 0.998 for CFO and NFO respectively, confirming the higher stability of the inverse spinel structure of NFO over CFO. Experimentally, it has indeed been reported that NFO crystals with a nearly perfect inverse spinel structure can be grown [89,90], while CFO samples are most of the time found with an inversion degree around 0.7–0.9 [58,59,90–92].

With the decrease of the inversion degree λ , we also calculated a linear increase of the pseudocubic lattice parameter $\langle a \rangle$, with a slope of -5.2 pm for NFO and of -5.3 pm for CFO, as shown in Fig. 3(b). Qualitative similar variations of $\langle a \rangle(\lambda)$ have been reported by Fritsch and Ederer [30], while opposite variations have been predicted in Ref. [29]. The linear decrease of $a(\lambda)$ is consistent with the equation proposed in Ref. [93,94], which expresses the variation of the lattice parameter as a function of the inversion parameter λ and of the ionic radii R of M^{2+} and Fe^{3+} cations,

$$a(\text{MFe}_2\text{O}_4) = \frac{8}{3\sqrt{3}}[(R_{\text{Td}} + R_{\text{O}}) + \sqrt{3}(R_{\text{Oh}} + R_{\text{O}})] \quad (9)$$

with $R_{\text{Td}} = (1 - \lambda)R_{\text{Co}^{2+}} + \lambda R_{\text{Fe}^{3+}}$ and $R_{\text{Oh}} = \frac{1}{2}[\lambda R_{\text{Co}^{2+}} + (2 - \lambda)R_{\text{Fe}^{3+}}]$. From this equation, the slope of the variation of $a(\lambda)$ is equal to $(1 - \frac{\sqrt{3}}{2})(R_{\text{Fe}^{3+}} - R_{M^{2+}})$, which is negative considering that $R_{\text{Fe}^{3+}} < R_{M^{2+}}$.

Finally, it is also interesting to mention that an auxetic behavior with an increase of the volume was measured for CFO samples with an inversion degree of approximately $\lambda = 0.75$; its origin is still not well understood, but is certainly related to the presence of cation or anion vacancies, in addition to the relatively high content of Co atoms in Td atomic sites [59]. Depending on the distribution of the Co atoms located in the occupied Td sites, our structure may not strictly preserve its slightly tetragonal shape. We calculated a small modification of the c/a ratio of CFO, from 0.995 to 0.998 when λ decreases from 1 to 0.875.

b. Magnetic properties. We calculated a linear decrease of the total spin magnetic moment per formula unit when the inversion parameter increases. It follows the equation:

$$M_{\text{f.u.}}(\text{MFe}_2\text{O}_4) = 2(1 - \lambda)M(\text{Fe}^{3+}) + (2\lambda - 1)M(M^{2+}) \quad (10)$$

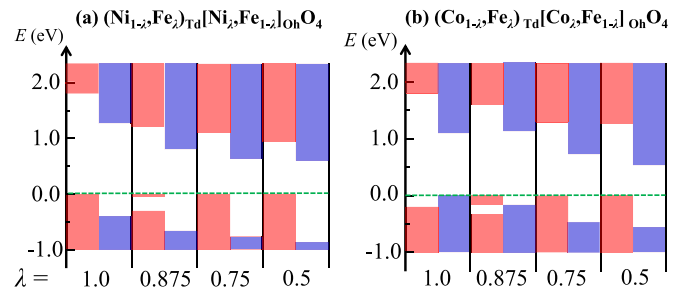


FIG. 4. Schematic representation of the density of states calculated (a) for NFO and (b) for CFO and for different values of the inversion degree λ . The energy range of the band gap corresponds to the white area. Minority- and majority-spin DOS are respectively shown with red and blue colors. The green dashed line corresponds to the highest occupied state.

Using the perfectly ionic model to describe CFO and NFO, which corresponds to the atomic spin magnetic moments $M(\text{Fe}^{3+}) = 5 \mu_B$, $M(\text{Co}^{2+}) = 3 \mu_B$ and $M(\text{Ni}^{2+}) = 2 \mu_B$, the previous equation becomes $M_{\text{f.u.}} = (-4\lambda + 7)\mu_B$ for CFO and $M_{\text{f.u.}} = (-6\lambda + 8)\mu_B$ for NFO.

We emphasize that the modifications of spin magnetic moments reported here have only been calculated approximately, as we restricted our study to a perfectly-collinear ferrimagnetic order. Recently, Moya *et al.* have shown that different values of the inversion parameter lead to different values of the total spin magnetic moment, due to a lowering of the magnetic coupling and to a canting of the cation magnetic moments, in particular for Co^{2+} cations. Two reasons were given by these authors to explain this effect: the first one is a direct consequence of the noninverse structure, with $\text{Co}^{2+}(\text{Td})\text{-O-Fe}^{3+}(\text{Oh})$ antiferromagnetic superexchange interactions lower than the dominant $\text{Fe}^{3+}(\text{Td})\text{-O-Fe}^{3+}(\text{Oh})$ ones; the second reason potentially comes from structural relaxations induced by other defects [95]. From our calculations (see Supplemental Material [43]), we indeed found that the antiferromagnetic coupling constant between cations in Oh and in Td atomic sites is reduced by 2–3 meV, for both CFO and NFO, when the inversion degree λ decreases from 1 to 0.875. As detailed in Sec. III A 1, from our calculations we found that the spin canting in CFO is relatively low for a perfectly inverse spinel structure. When the structure is partially inverse ($\lambda = 0.875$), the magnitude of the spin cantings remains of the same magnitude and the total spin magnetic moment undergoes a decrease by 0.2% of the same order than for $\lambda = 1$.

c. Electronic structure. As shown in Fig. 4, replacing $\text{Fe}^{3+}(d^5)$ cations by $\text{Co}^{2+}(d^7)$ or $\text{Ni}^{2+}(d^8)$ in Td sites will create occupied defect states in the majority-spin band gap, the sign of the magnetic moment of the cations in Td sites being opposite to that of the other cations. Jointly, adding more $\text{Fe}^{3+}(d^5)$ cations in Oh sites will depopulate the minority-spin bands and unoccupied gap states will appear. In summary, when the inversion degree decreases, the minority-spin bands are less occupied for the benefit of the occupation of majority-spin bands and both occupied and unoccupied gap states will merge with the bulk continuum of valence and conduction bands when the inversion degree is too low. This leads for

instance to a decrease of the spin-dependent band gaps of 29% for NFO and of 6% for CFO for $\lambda = 0.5$ in comparison to the perfectly inverse structures; the fundamental band gap displays a larger decrease by 70% for NFO and by 55% for CFO. For CFO, it is finally interesting to note that for $\lambda \neq 1$, the VBM does not belong to the minority-spin channel anymore.

B. Physical properties of nonstoichiometric CFO and NFO crystals

We now describe the consequences on the physical properties of CFO and NFO of several kinds of point defects that modify the stoichiometry of these crystals. We will start exploring cation substitutions leading to a Fe:(Co,Ni) ratio different from 2. Such defects are very likely to exist, owing to the difficulty to precisely control the global and local stoichiometry of CoFe_2O_4 and NiFe_2O_4 samples. A Fe:(Co,Ni) ratio different from 2 can also arise due to the presence of cation vacancies, another kind of point defects that we have chosen to consider in this paper. Cation vacancies are common defects in spinel ferrites, which can even lead to metastable cation-deficient spinel structures, such as maghemite $\gamma\text{-Fe}_2\text{O}_3$ [96], which can be described as a Fe-deficient magnetite crystal. Recent experimental and numerical studies [18,33] focused on cation diffusion, which can even be controlled by applying an external electric field, and which could also be promoted by the presence of either oxygen or cation vacancies [18]. Oxygen vacancies are the last kind of point defects that we will address in this section: Up to now, the existence of oxygen vacancies has mostly been hypothesized to explain the measured modification of the magnetization and electrical conductivity.

1. Effects of cation substitutions

We first describe the physical properties of the spinel ferrites $M_{1-\alpha}\text{Fe}_{2+\alpha}\text{O}_4$ ($\alpha > 0$), in which some of the $M = (\text{Co}, \text{Ni})$ atoms have been replaced by Fe and $M_{1+\beta}\text{Fe}_{2-\beta}\text{O}_4$ ($\beta > 0$), in which part of the Fe have been replaced by M atoms.

a. Atomic structure. For $M_{1+\beta}\text{Fe}_{2-\beta}\text{O}_4$, we only considered the substitution of Fe atoms by Co or Ni atoms occurring in Oh sites: This scenario appeared to be the most probable one, according to the results presented in the previous section and it has also been confirmed by a comparison of the total energies that we calculated. Indeed, we found that substituting a single Fe atom in a Td site of the conventional cell containing 8 $M\text{Fe}_2\text{O}_4$ f.u. costs 1.403 eV and 1.568 eV more, respectively for CFO and NFO, than when the substitution involves an Fe atom located in one of the Oh sites.

Whatever the Oh site in which the substitution occurs, we found that the cell tends to become more cubic after this substitution, with a c/a ratio closer to 1. The averaged lattice parameter does not change significantly when Fe is replaced by Co atoms, while it tends to decrease when Co is replaced by Fe atoms in CFO. For NFO, substituting Fe by Ni atoms increases the lattice parameter ($\langle a \rangle = 0.8295$ nm for $\beta = 0.125$ and 0.8301 nm for $\beta = 0.25$), while replacing Ni by Fe atoms decreases $\langle a \rangle$ to 0.8282 nm for $\alpha = 0.125$ and 0.8262 nm for $\alpha = 0.25$.

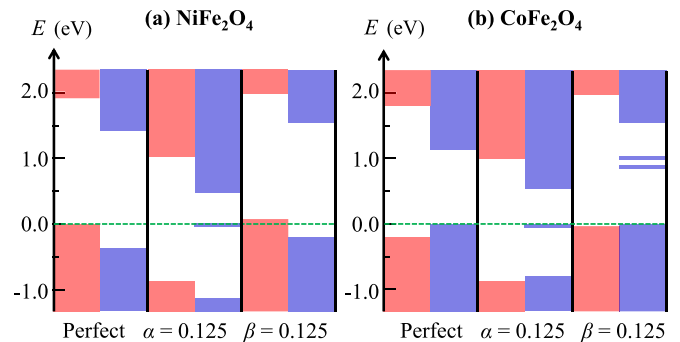


FIG. 5. Same as in Fig. 4, but for the nonstoichiometric crystals $M_{0.875}\text{Fe}_{2.125}\text{O}_4$ ($\alpha = 0.125$) and $M_{1.125}\text{Fe}_{1.875}\text{O}_4$ ($\beta = 0.125$).

b. Electronic structure. As it can be seen in Fig. 5, substituting Ni or Co by Fe atoms has a very similar effect in both compounds: it creates occupied minority-spin states near the middle of the band gap. The fact that these gap states are occupied means that Fe replacing Ni or Co atoms in Oh sites are Fe^{2+} cations. The ferrite crystal can then be described by the chemical formula $(\text{Fe}^{3+})_{\text{Td}}[\text{M}_{1-\alpha}^{2+}\text{Fe}_{\alpha}^{2+}\text{Fe}^{3+}]_{\text{Oh}}\text{O}_4^{2-}$.

Conversely, substituting Fe by M atoms leads to the formation of M^{3+} cations in order to preserve the charge neutrality of the crystal, which can further be described by the chemical formula $(\text{Fe}^{3+})_{\text{Td}}[\text{M}^{2+}\text{M}_{\beta}^{3+}\text{Fe}_{1-\beta}^{3+}]_{\text{Oh}}\text{O}_4^{2-}$, with $\beta > 0$. We have observed some differences between the results that we calculated for NFO and CFO: for CFO, the Co^{3+} replacing Fe^{3+} cations have a $d_{\uparrow}^5 d_{\downarrow}^1$ electronic structure and the unoccupied minority spin gap states have an energy near the middle of the band-gap, while for NFO the Ni^{3+} cations are in a $d_{\uparrow}^4 d_{\downarrow}^3$ low-spin state and the VBM in the majority-spin channel will be depopulated and will cross the Fermi level. The depopulated bands have a $(d_{x^2-y^2} + d_{z^2} + p_z)$ character and an effective mass $m_h = 1.55m_0$.

c. Magnetic properties. The changes in the electronic structure described just before are consistent with the calculated total magnetic moments. The corresponding total spin magnetic moment of a $M\text{Fe}_2\text{O}_4$ crystal with an iron over-stoichiometry ($\alpha > 0$) is thus given, in the ionic approximation, by the equation

$$M_{\text{f.u.}}(M_{1-\alpha}\text{Fe}_{2+\alpha}\text{O}_4) = (1 - \alpha)M(M^{2+}) + \alpha M(\text{Fe}^{2+}) \quad (11)$$

which leads to $M_{\text{f.u.}}(\text{Ni}_{1-\alpha}\text{Fe}_{2+\alpha}\text{O}_4) = 2(\alpha + 1) \mu_B$ and $M_{\text{f.u.}}(\text{Co}_{1-\alpha}\text{Fe}_{2+\alpha}\text{O}_4) = (\alpha + 3) \mu_B$, in perfect agreement with our DFT results.

On the contrary, when there is an excess of Co or Ni atoms ($\beta > 0$), the spin magnetic moment per formula unit is given, in the ionic approximation, by

$$M_{\text{f.u.}}(M_{1+\beta}\text{Fe}_{2-\beta}\text{O}_4) = M(M^{2+}) + \beta[M(M^{3+}) - M(\text{Fe}^{3+})] \quad (12)$$

with $M(\text{Co}^{3+}) = 4 \mu_B$ and $M(\text{Ni}^{3+}) = 1 \mu_B$ (in low-spin state). This equation leads to $M_{\text{f.u.}}(\text{Ni}_{1+\beta}\text{Fe}_{2-\beta}\text{O}_4) = (2 - 4\beta) \mu_B$ and $M_{\text{f.u.}}(\text{Co}_{1+\beta}\text{Fe}_{2-\beta}\text{O}_4) = (3 - \beta) \mu_B$, respectively for nonstoichiometric NFO and CFO.

In conclusion, we predicted from our calculations that increasing the amount of Fe atoms by substituting Ni or Co atoms will lead to an increase of the total magnetic moment,

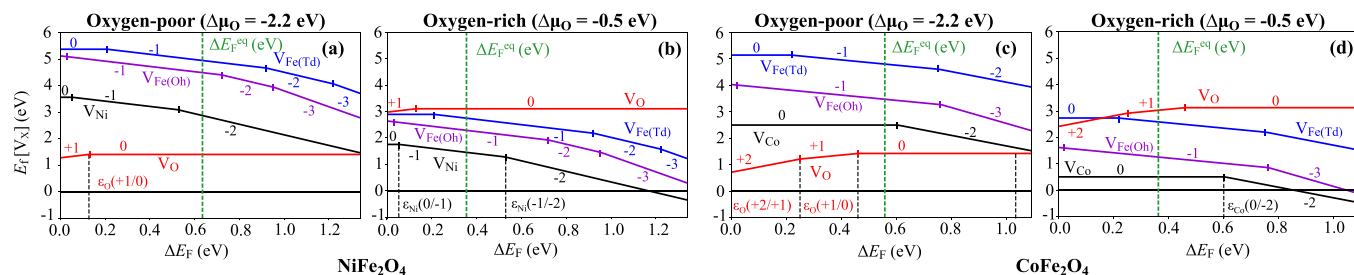


FIG. 6. Formation energies $E_f[V_X^q]$ of charged atom vacancies in NFO for (a) the oxygen-poor conditions ($\Delta\mu_O = -2.2$ eV) and (b) for the oxygen-rich conditions ($\Delta\mu_O = -0.5$ eV). Formation energies of charged atom vacancies in CFO under similar oxygen-poor and oxygen-rich conditions are respectively given in the panels (c) and (d). The formation energies are given as a function of the position of the Fermi level ΔE_F , which is given with respect to the VBM of the perfect bulk compounds. Only the energies corresponding to the most stable charge states q of each kind of vacancies are shown and these charge states are indicated. The green lines indicate the equilibrium Fermi level $\Delta E_F^{\text{eq}}(T_g, T_R)$ calculated according to the equations and temperatures given in Sec. II.

while on the contrary, substituting Fe atoms by Ni or Co atoms will decrease it.

2. Effects of atom vacancies

In this section, we discuss the effects of cation and oxygen vacancies on the electronic structure and on the magnetic properties of CFO and NFO. We studied the oxygen-deficient ferrites $(\text{Fe})_{\text{Td}}[\text{MFe}]_{\text{Oh}}\text{O}_{4-\zeta}$ and the metal-deficient compounds $(\text{Fe})_{\text{Td}}[\text{M}_{1-\gamma}\text{Fe}]_{\text{Oh}}\text{O}_4$, $(\text{Fe})_{\text{Td}}[\text{MFe}_{1-\delta}]_{\text{Oh}}\text{O}_4$ and $(\text{Fe}_{1-\epsilon})_{\text{Td}}(\text{MFe})_{\text{Oh}}\text{O}_4$. Some of these defects have already been studied in spinel ferrites such as Fe_3O_4 [26,27] or NiFe_2O_4 [97].

a. Thermodynamic stability. The vacancy formation energies $E_f[V_X^q]$ have been calculated using Eq. (1) for different values of the chemical potentials $\Delta\mu_X$ within the ranges where CFO and NFO can exist as stable compounds (see the phase diagrams of the two oxides in Appendix). For each spinel oxide, we will focus our discussions on oxygen-rich ($\Delta\mu_O = -0.5$ eV) and oxygen-poor ($\Delta\mu_O = -2.2$ eV) growth conditions.

According to Eq. (1), the vacancy formation energies depend on the value of the electronic chemical potential qE_F , which itself depends on the concentration of all the possible (charged) defects. Note that E_F can also depend on the presence of space charges and can be tuned experimentally by varying the temperature or by applying an electric field, when the spinel ferrite oxide is one of the constituent layers of an electronic device.

Figure 6 shows the values of the formation energies $E_f[V_X^q]$ calculated for the different kinds of atom vacancies in NFO and CFO and as a function of $\Delta E_F = E_F - E_{\text{VBM}}^H$, which varies within the fundamental band gap of these oxides. An equilibrium Fermi level $\Delta E_F^{\text{eq}}(T_g, T_R)$, computed from Eqs. (3)–(7), is also given.

For both oxides and under oxygen-poor growth conditions, the formation energy of the oxygen and cation vacancies are all positive, whatever the values taken by ΔE_F within the band gap. These defects are thus unlikely to be formed when CFO and NFO are grown at low temperature. When the growth temperature increases, due to the exponential factor in Eq. (6), the concentration of the atom vacancies with the lowest formation energy will be definitively greater than that of the other kinds of vacancies.

For NFO, the most probable defects under oxygen-poor growth conditions will thus be: V_{Ni}^{-2} for $\Delta E_F > 1.37$ eV (i.e., when ΔE_F is 0.03 eV higher than the calculated band gap), V_{O}^0 for $0.13 < \Delta E_F < 1.37$ eV and V_{O}^{+1} for $0 < \Delta E_F < 0.13$ eV. V_{O}^0 and V_{O}^{+1} should coexist with similar concentrations for $\Delta E_F \approx 0.13$ eV. At the calculated equilibrium Fermi level $\Delta E_F^{\text{eq}} = 0.64$ eV, we expect mainly to observe V_{O}^0 vacancies, with a calculated concentration $[V_{\text{O}}^0] = 1.2 \times 10^{12} \text{ cm}^{-3}$, while ionized vacancies will be only present with a concentration of $[V_{\text{O}}^{+1}] = 9 \times 10^2 \text{ cm}^{-3}$. The calculated equilibrium Fermi level being close to the middle of the gap, the numbers of free holes and electrons is balanced to $n = p = 4 \times 10^8 \text{ cm}^{-3}$. For CFO under oxygen-poor growth conditions, the most probable defects are V_{Co}^{-2} for $\Delta E_F > 1.14$ eV (i.e., 0.05 eV above E_g) and oxygen vacancies for $\Delta E_F < 1.14$ eV. The two ionization energies for charge-state transitions are $\varepsilon(+1/0) = 0.46$ eV and $\varepsilon(+2/+1) = 0.25$ eV. At the equilibrium Fermi level $\Delta E_F^{\text{eq}} = 0.56$ eV, as in NFO, we also have mostly the presence of neutral oxygen vacancies with a similar concentration of $[V_{\text{O}}^0] = 1.2 \times 10^{12} \text{ cm}^{-3}$, 9 orders of magnitude higher than the concentration of Co vacancies. In CFO, the concentration of free carriers $n \simeq p = 2.6 \times 10^{10} \text{ cm}^{-3}$ is higher than in NFO.

Ni/Co vacancies will be the most stable defects under oxygen-rich conditions. For NFO, these conditions allowed to calculate a Fermi level of $\Delta E_F^{\text{eq}} = 0.35$ eV, for which the Ni vacancies will be mostly partially ionized ($q = -1$), with a concentration $[V_{\text{Ni}}^{-1}] = 2 \times 10^{13} \text{ cm}^{-3}$. At this Fermi level, the concentration of neutral or fully-ionized Ni vacancies, even if 3 to 5 orders of magnitude lower, is however not negligible; Fe(Oh) vacancies will also be present. For CFO, we have $\Delta E_F^{\text{eq}} = 0.36$ eV (which is below the critical value of $\varepsilon(0/-2) = 0.60$ eV at which cobalt vacancies with $q = 0$ and $q = -2$ are equally probable) and the Co vacancies will mostly be neutral, with a very high concentration of $[V_{\text{Co}}^0] = 3 \times 10^{18} \text{ cm}^{-3}$. Other defects are present with the concentrations ($[V_{\text{Co}}^{-2}], [V_{\text{Co}}^{-1}], [V_{\text{Fe(Oh)}}^{-1}]$) $\sim 10^{10}$ – 10^{13} cm^{-3} . Oxygen-rich conditions, for both CFO and NFO, the Fermi level is calculated closer from the VBM than in oxygen-poor conditions, and we thus have a larger amount of free holes ($p = 2$ – $4 \times 10^{13} \text{ cm}^{-3}$).

Additional comments can be made on the formation energies of the different defects. First, if we predicted that we

will mostly observe Ni or Co vacancies in oxygen-rich conditions, the formation of Fe_{Oh} vacancies cannot totally be excluded, as their formation energy can be close to those of Co/Ni vacancies when the Fermi level approaches the CBM (these vacancies can even become the most stable ones under Fe-poor conditions). Secondly, for all the studied cases, Fe_{Td} vacancies are always the less stable cation vacancies, in agreement with former calculations performed on iron-deficient Fe_3O_4 [27]. More details about the calculated vacancy concentrations can be found in Table VII in the Supplemental Material [43]. Thirdly, still in oxygen-rich conditions, we can see that when the Fermi level is close to the CBM, the formation energies $E_f[V_{\text{Fe(Oh)}}^{-3}]$ and $E_f[V_{\text{M(Oh)}}^{-2}]$ become negative and these defects can appear spontaneously, even at low temperature. In oxygen-poor conditions such that the Fermi level approaches the CBM will favor a coexistence of Co/Ni and O vacancies.

Studying the coexistence of several kinds of vacancies in the same sample is beyond the scope of the current paper. However, we performed a preliminary calculation on a neutral Ni-O bivacancy created in a supercell containing 8 f.u. of NFO and considering oxygen-poor growth conditions. When both vacancies are as close as possible, i.e., separated by a distance of approximately 2 Å, the formation energy of this complex defect is of 3.38 eV. If we take the two vacancies away, separated by a distance of 4.6 Å, the formation energy increases by 0.3 eV. The energy increases up to 1.7 eV when we consider the sum of the two formation energies calculated for the isolated neutral or $+1/-1$ -charged Ni and O vacancies, that is $E_f[V_{\text{Ni}}^0] + E_f[V_{\text{O}}^0]$ or $E_f[V_{\text{Ni}}^{-1}] + E_f[V_{\text{O}}^{+1}]$. Such a neutral bivacancy does not lead to electronic reconstructions, the oxidation degrees of Ni and O ions canceling out each other, which may explain the defect stability.

Our results on vacancies could help explaining some of the experimental studies that aim either at understanding the effects of structural defects in spinel ferrites, or at manipulating the structure of these oxides to reach specific functional properties. This is, for instance, the case of the study reported by Chen, *et al.*, who succeeded in reversing the magnetization of an iron-deficient CoFe_2O_4 sample by applying an electric field [18]. Their study highlights the role of the Co-atom migration, in agreement with our calculations, which demonstrates that Co vacancies are among the easiest defects to be formed. The authors of this paper also discussed the role of oxygen vacancies in promoting the formation of adjacent iron vacancies and facilitating Co migration, which is also discussed in Ref. [19]. A numerical study of ion migration in spinel ferrites has been reported in Ref. [33]: In comparison with NFO, higher diffusion speeds and lower barrier activation energies have been calculated by these authors for CFO. This partly results from the larger lattice parameter of CFO. In our paper, we also found that Co vacancies have lower formation energies than Ni vacancies in oxygen-rich growth conditions.

b. Atomic structure. The presence of a neutral cation vacancy in the conventional cell systematically lowers the averaged lattice parameter $\langle a \rangle$ of NFO by 1.4 to 3.6 pm. Conversely, the lattice parameter increases up to 11.7 pm when the charge state q of the cation vacancy decreases. The presence of a Ni vacancy in the cell also increases the ratio c/a to 1.012, which could enhance the electric polarization

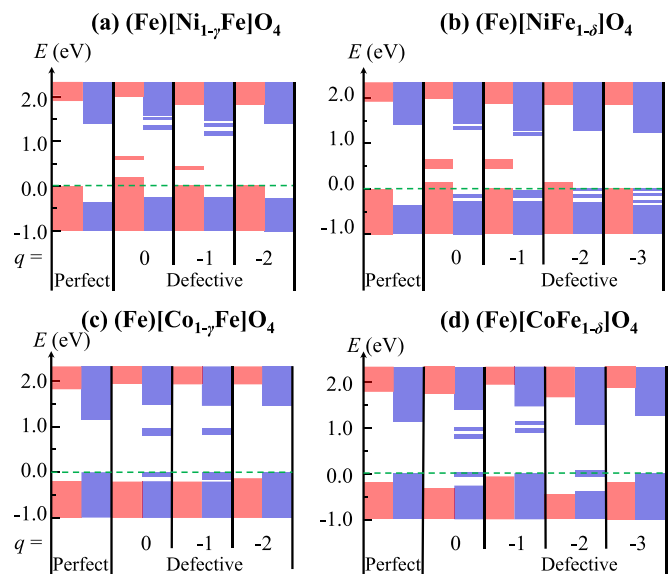


FIG. 7. Same as in Fig. 4, but for [(a),(b)] NFO and [(c),(d)] CFO crystals with different cations vacancies and different charge states q .

of the oxide. Fe(Td) vacancies are the defects that induce the strongest variations of the pseudocubic lattice parameter, changing the structure from tetragonal to orthorhombic. Similar conclusions are observed for CFO, except for the increase of the tetragonality of the cell, which is not induced by Co vacancies. Oxygen vacancies have only small effects on the pseudocubic lattice parameter $\langle a \rangle$ of CFO, even when these defects are charged, while increasing the charge state q of oxygen vacancies increases $\langle a \rangle$ up to 1% for $q = +2$ in NFO.

c. Electronic structure. Our results show that a cation vacancy enhances the valence state of the Co and Ni cations the closest from this defect. This enhancement depends on the charge state of the vacancy. Conversely, an oxygen vacancy will lower the valence state of the surrounding Fe cations.

A neutral cation vacancy V^0 induces an electronic reconstruction, with the transfer of holes to the Co or Ni cations first-neighbors of the vacancy. As shown in Fig. 7, these holes will be generated by depopulating the highest occupied orbitals, which have e_g -like (t_{2g} -like) symmetries and belong to the majority (minority) spin channel for NFO (CFO), thus creating gap states in the same spin channel. When a cation vacancy is charged, the number of transferred holes decreases, down to 0 for both $V_{\text{M(Oh)}}^{-2}$ or $V_{\text{Fe(Oh)}}^{-3}$. If the electronic reconstruction induced by the defects only implies one hole, this hole is mainly localized in the cations first neighbors of the vacancy. When more holes are transferred (for neutral vacancies in particular), we observe a delocalization over more Ni/Co cations (which is reflected on the variation of spin magnetic moments of Ni cations, as shown in Fig. 2 in the Supplemental Material [43]). The top of the valence band of NFO even crosses the Fermi level for the specific defects $V_{\text{Ni(Oh)}}^0$, $V_{\text{Fe(Oh)}}^0$, and $V_{\text{Fe(Oh)}}^{-2}$. We remind that neutral cation vacancies are the most stable when the Fermi level is close to the VBM; such a condition would favor p doping in NFO. Finally, we can notice that occupied gap states are also induced by Fe vacancies, both in CFO and in NFO and their existence is certainly due to the presence of dangling chemical bonds.

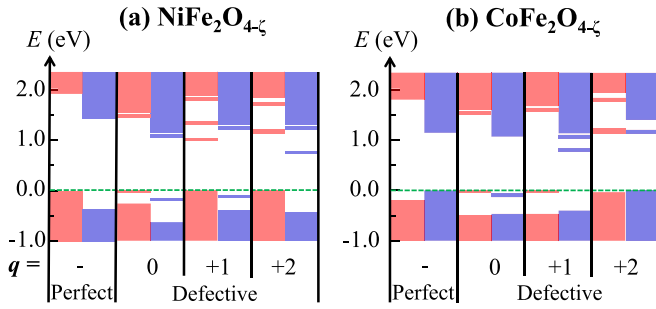


FIG. 8. Same as in Fig. 4, but for oxygen-deficient (a) NFO and (b) CFO crystals.

Under oxygen-poor growth conditions, oxygen vacancies will most likely exist with the charge state $q = 0$. Their presence goes along with an electronic reconstruction, an occupied state appearing in the majority spin channel and another one in the minority spin channel (Fig. 8). Ionized oxygen vacancies can be formed when the Fermi level is close to the VBM. Oxygen vacancies with the charge state $q = +2$ do not lead to a charge imbalance and to an electronic reconstruction. When the charge state of the oxygen vacancy is $q = +1$, which may happen when the Fermi level is close to the VBM, a single occupied gap state appears in the majority-spin channel for CFO and minority-spin channel for NFO.

d. Magnetic properties. As discussed in a former study on Fe_3O_4 [27], the variation of total spin magnetic moment induced by vacancies in a spinel ferrite crystal can be decomposed in two different contributions, which are

(1) A decrease(increase) of its value due to the removal of atoms in Oh(Td) atomic sites

(2) Its potential increase(decrease) due to the electronic reconstruction, as already discussed in the previous paragraph.

In an oxygen-rich environment, when mostly cation vacancies with the charge state q are created, we can use $M(\text{Co}^{2+}) = 3 \mu_B$, $M(\text{Ni}^{2+}) = 2 \mu_B$ and $M(\text{Fe}^{3+}) = 5 \mu_B$ and the following equations to explain the values of the spin magnetic moment per formula unit that we calculated from first principles:

$$M_{\text{f.u.}}(\text{Co}_{1-\gamma}\text{Fe}_2\text{O}_4) = (1 - \gamma)M(\text{Co}^{2+}) + [(2 - |q|)\gamma]\mu_B \quad (13)$$

i.e., $M_{\text{f.u.}} = [3 - (1 + |q|)\gamma] \mu_B$ for $\text{Co}_{1-\gamma}\text{Fe}_2\text{O}_4$, if we consider that only Co vacancies can be stable in CFO and

$$M_{\text{f.u.}}(\text{Ni}_{1-\gamma}\text{Fe}_2\text{O}_4) = (1 - \gamma)M(\text{Ni}^{2+}) + [(|q| - 2)\gamma]\mu_B \quad (14)$$

i.e., $M_{\text{f.u.}} = [(|q| - 4)\gamma + 2] \mu_B$ for $\text{Ni}_{1-\gamma}\text{Fe}_2\text{O}_4$, when only Ni vacancies are present. In iron-poor conditions, we also expect the following value of the spin magnetic moment:

$$M_{\text{f.u.}}(\text{NiFe}_{2-\delta}\text{O}_4) = M(\text{Ni}^{2+}) - \delta M(\text{Fe}^{3+}) + [(|q| - 3)\delta]\mu_B \quad (15)$$

i.e., $M_{\text{f.u.}} = [(|q| - 8)\delta + 2] \mu_B$ for $\text{NiFe}_{2-\delta}\text{O}_4$, with only Fe_{Oh} vacancies.

According to our first-principles results, these equations, which should be used at low vacancy contents, hold at least up to $\gamma, \delta = 1/8$. For higher vacancy contents, these equations may not be valid anymore: the stoichiometry being too different from that of $M\text{Fe}_2\text{O}_4$, other compounds should

stabilize. Because the charge state q of a cation vacancy can be at most -3 and because vacancies are most likely to be found in Oh sites, our analysis thus predicts a systematic decrease of the magnetization due to the presence of such defects.

Let us now consider the effects of oxygen vacancies. Oxygen being a nonmagnetic atom, changes in total magnetic moments can only be induced by the redistribution of charges for neutral or partially ionized vacancies. As discussed before, no electronic reconstruction will occur for $q = +2$. For $q = 0$, one additional electron is transferred in each spin channel: One electron onto the Fe_{Td} atom first-neighbor of the vacancy, while the other one is spread among Fe_{Oh} atoms, and stays mostly localized near the vacancy. These two charge transfers induce local decreases of the spin magnetic moments (see Fig. 2 in the Supplemental Material [43]), which compensate for each other on average (Fe_{Td} and Fe_{Oh} atoms being antiferromagnetically coupled) and leave the total spin magnetic moment unchanged for both materials, in agreement with previous predictions reported on Fe_3O_4 [26]. Other reported calculations tend however to predict the transfer of electrons only in the minority-spin channel [97]. In summary, V_{O}^{+2} and V_{O}^0 vacancies should not be considered as responsible for a noticeable change in the magnetization,

$$M_{\text{f.u.}} = M(M_{\text{Oh}}^{2+}) \quad (16)$$

if $q = 0, +2$

For $q = +1$, which is less probable, we do not have the same compensation of the magnetic moments as for $q = 0$: only one electron will be transferred to Fe^{3+} cations located in Td sites for CFO and in Oh sites for NFO.

Our calculations show that an oxygen vacancy does not induce a direct change of the total spin magnetic moment, unless its charge state is $q = +1$. In this case, the total spin magnetic moment of the NFO(CFO) crystal will thus decrease(increase) by $\zeta \mu_B$,

$$\begin{aligned} M_{\text{f.u.}}(\text{NFO}) &= M(\text{Ni}_{\text{Oh}}^{2+}) + \zeta [M(\text{Fe}_{\text{Oh}}^{2+}) - M(\text{Fe}_{\text{Oh}}^{3+})] \\ &= (2 - \zeta) \mu_B, \\ M_{\text{f.u.}}(\text{CFO}) &= M(\text{Co}_{\text{Oh}}^{2+}) + \zeta [M(\text{Fe}_{\text{Td}}^{2+}) - M(\text{Fe}_{\text{Td}}^{3+})] \\ &= (3 + \zeta) \mu_B. \end{aligned} \quad (17)$$

In addition to our numerical results, it is important to mention that real samples may be more complex. Munjal and Khare [20], who studied resistive and magnetization switching as a function of an applied electric field, used x-ray photoelectron spectroscopy to measure changes in the oxidation state of Co cations, from Co^{2+} to Co^0 . They did not observe the modification of the oxidation state of iron cations, suggesting that this may occur due to the easiest formation of oxygen vacancies near Co than near Fe atoms. Robbenolt, *et al.* also identified the formation of Co^0 atoms, with a smaller concentration of Fe^0 when a sufficiently large voltage is applied on mesoporous CFO [21]. The discrepancy between this experimental study and our calculations may also confirm the necessity to extend our work to the more systematic study of multiple vacancies, as such experimental observations may be the result of the presence of several oxygen vacancies in Co-rich areas.

IV. CONCLUSIONS

We performed a detailed study of the variations of the atomic, electronic and magnetic properties of the spinel ferrites CoFe_2O_4 and NiFe_2O_4 induced by different kinds of structural point defects. We considered separately the effects of cation ordering in stoichiometric structures and of the non-stoichiometry arising from cation substitutions or from the presence of vacancies. Our main conclusions are the following:

(1) The $P4_122$ space group is found to be the most stable for the inverse spinel ferrite NFO and the second most stable one for CFO. For this latter compound, another space group ($P2/c$) was identified as more stable, but this remains to be confirmed.

(2) Inverse cation distribution is more robust in NFO than in CFO. The perfectly inverse spinel structure has the lowest total magnetic moment of $3\mu_B$ for CFO and of $2\mu_B$ for NFO, and the magnetization increases when the inversion degree decreases, i.e., when the structure tends to become that of a normal spinel. Both ferrites remain insulating when the inversion parameter is between 0.5 and 1, but their fundamental band gap is strongly reduced. Combined with other defects in reductive environment, the decrease of the inversion parameter would thus favor the appearance of conductivity.

(3) Co/Ni, Fe(Oh) or O vacancies (depending on the growth conditions) are found to be the most probable defects. Only the presence of cation vacancies is expected to greatly decrease the magnetization (this decrease depending on the vacancy ionization state) while, according to our calculations, no or only few magnetization changes should originate from oxygen vacancies.

(4) Cation vacancies will be responsible for a transfer of holes to the VBM of the crystal, in the majority-spin channel for NFO and in the minority-spin channel for CFO, because of the different spin orientation of the VBM for the two perfect materials. p-doping with a Ni/Fe ratio over 1/2 can also induce the formation of Ni^{3+} cations with gap states very close to the bulk VBM. In the case where Ni cations substitute Fe cations in Oh sites, we observed the formation of Ni^{3+} cations with a low-spin state, which promotes a half-metallic state with a fully-spin-polarized hole conductivity.

As mentioned throughout the paper, different open questions remain and several perspectives could be proposed to our study.

Among the most important points, we only considered single and isolated defects. However, real samples generally possess combinations of these defects and their mutual interaction is not well understood. We have shown for example that a neutral Ni-O bi-vacancy is more stable than the separated Ni and O vacancies, which may be partly explained by the compensating oxidation number of the corresponding ions. The interaction between vacancies and cation distribution would also deserve a deep investigation. In particular, as discussed at the end of this paper, the experimental observation of Co^0 or Fe^0 atoms [20,21] in a sample, which cannot be explained by our calculations, and preferential sites for the formation of oxygen vacancies, leading to inhomogeneities,

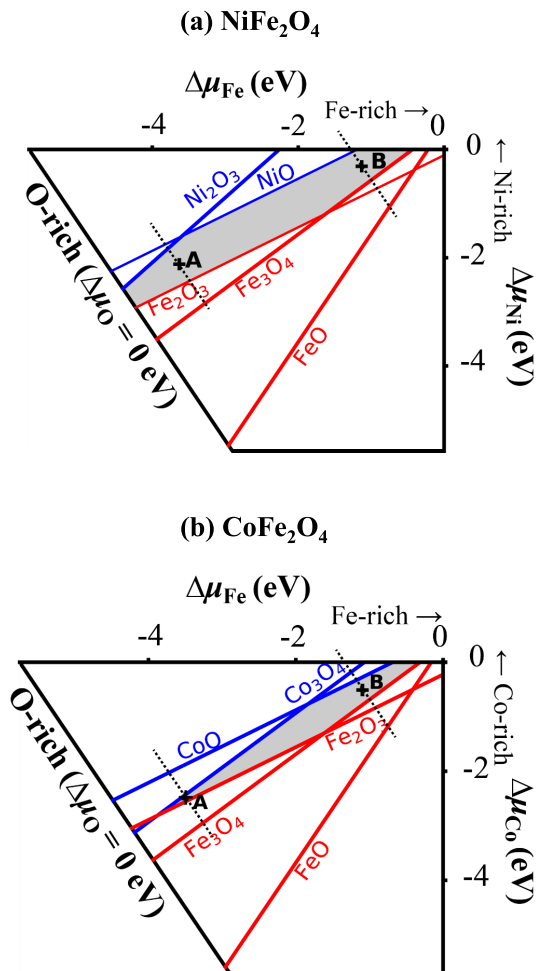


FIG. 9. Stability phase diagrams of (a) NFO and (b) CFO. The chemical potential ranges where CFO and NFO are more stable than competing phases are shown by shaded areas. A and B points are median values for oxygen-rich ($\Delta\mu_{\text{O}} = -0.5$ eV) and oxygen-poor ($\Delta\mu_{\text{O}} = -2.2$ eV) conditions respectively.

should be considered. We also mentioned that p-doping by specific defects could induce the appearance of spin-polarized holes in the VBM of NFO or CFO. In the case of CFO the spin orientation of the VBM depends on the inversion degree: Associating both contributions could certainly alter our results. Another natural extension of this paper would also consist in combining the study of point defects with the study of extended defects (like antiphase boundaries which are common in these compounds), of strain effects (which can change both the cation distribution [30] and the formation energy of the vacancies), or also of interfaces.

Finally, the effect of point defects on other material properties is also a possible way to pursue this study. In addition to the magnetization, the electric polarization evidenced in NiFe_2O_4 [71,76] is expected to depend on the cation distribution, but can also be affected by the presence of vacancies, which could lead to tunable magnetoelectric effects. The calculated dependence of the c/a ratio and also of the conductive behavior over different defects discussed in this paper may give a first clue of the importance of taking them into account.

ACKNOWLEDGMENTS

This study has been supported through the ANR Grant No. ANR-19-CE09-0036. This work was granted access to the HPC resources of CALMIP (Allocation No. 2021-2022/P19004 and P1229).

APPENDIX: STABILITY PHASE DIAGRAMS

To calculate the formation energy of the vacancies from Eq. (1), it is necessary to determine the energy range of the chemical potentials $\mu_i = E_i^{\text{elem}} + \Delta\mu_i$. To do so, we need first to introduce the formation enthalpy of the spinel ferrite $\Delta_f H(M\text{Fe}_2\text{O}_4)$:

$$\Delta_f H(M\text{Fe}_2\text{O}_4) = E_{M\text{Fe}_2\text{O}_4}^{\text{bulk}} - \sum_i N_i E_i^{\text{elem}} \quad (\text{A1})$$

where $E_{M\text{Fe}_2\text{O}_4}^{\text{bulk}}$ is the ground-state energy calculated for the $M\text{Fe}_2\text{O}_4$ spinel ferrite, E_i^{elem} are the total energies of the $M = \text{Co}/\text{Ni}$, Fe and O atoms in their pure solid or gas phases and N_i are the numbers of atoms of each chemical species in the compound chemical formula. The energies E_i^{elem} have been calculated according to the fitted elemental phase reference energy (FERE) method [98]; details on this method and a comparison of the atom energies calculated with other methods are given in the Supplemental materials [43].

Equation (A1) can be also written as a function of $\Delta\mu_i$:

$$\Delta\mu_M + 2\Delta\mu_{\text{Fe}} + 4\Delta\mu_{\text{O}} = \Delta_f H(M\text{Fe}_2\text{O}_4) \quad (\text{A2})$$

In the same way, to avoid the formation of any competitive phase $M_x\text{Fe}_y\text{O}_z$, the following inequalities have to be fulfilled:

$$n_x \Delta\mu_M + n_y \Delta\mu_{\text{Fe}} + n_z \Delta\mu_{\text{O}} \leq \Delta_f H(M_x\text{Fe}_y\text{O}_z) \quad (\text{A3})$$

From Eqs. (A1)–(A3), it is thus possible to calculate the phase diagrams plotted in Fig. 9, where we can see the

$\Delta\mu_i$ -stability domain of NFO and CFO (shaded areas). For NFO, our calculations are in fairly good agreement with those of Rák, *et al.* [99]. In Fig. 9, each point corresponds to a triplet $(\Delta\mu_{\text{Fe}}, \Delta\mu_M, \Delta\mu_{\text{O}})$. The points A and B, which have been chosen to express respectively an oxygen-rich and an oxygen-poor growth conditions have for coordinates $(-3.50, -2.50, -0.50)$ and $(-1.09, -0.51, -2.20)$ for CFO and $(-3.63, -2.12, -0.50)$ and $(-1.13, -0.31, -2.20)$ for NFO.

Interestingly, it is possible to express the chemical potential of oxygen atoms as a function of experimental growth conditions [100,101],

$$\Delta\mu_{\text{O}}(T, P) = \frac{1}{2} \{ [H_0 + \Delta H(T)] - T[S_0 + \Delta S(T)] \} + \frac{1}{2} k_B T \ln \left(\frac{P}{P_0} \right) \quad (\text{A4})$$

where $\Delta H(T) = C_p(T - T_0)$, $\Delta S(T) = C_p \ln(T/T_0)$. $H_0 = 8.7 \text{ kJ mol}^{-1}$, $S_0 = 205 \text{ J mol}^{-1} \text{ K}^{-1}$ are tabulated values [100,102] and $P_0 = 1 \text{ atm}$ and $T_0 = 298 \text{ K}$ are standard pressure and temperature.

From these equations, taking experimental growth conditions such as $T = 450 \text{ }^\circ\text{C}$ and $P = 10^{-10} \text{ mbar}$ [58], used to grow thin films of CFO, we obtain $\Delta\mu_{\text{O}}(T, P) = -1.69 \text{ eV}$, while $T = 400 \text{ }^\circ\text{C}$ and $P = 0.5 \text{ mbar}$ conditions have been used to grow CFO nanoparticles [59], corresponding then to $\Delta\mu_{\text{O}}(T, P) = -0.92 \text{ eV}$. As another example, the role of oxygen vacancies was also studied in NFO thin films [103] grown under a temperature of $T = 400 \text{ }^\circ\text{C}$ and an oxygen partial pressure of $P = 1.3 \times 10^{-6} \text{ mbar}$, which corresponds to a chemical potential $\Delta\mu_{\text{O}}(T, P) = -1.29 \text{ eV}$.

-
- [1] M. Coll, J. Fontcuberta, M. Althammer, M. Bibes, H. Boschker, A. Calleja, G. Cheng, M. Cuoco, R. Dittmann, B. Dkhil *et al.*, Towards oxide electronics: A roadmap, *Appl. Surf. Sci.* **482**, 1 (2019).
- [2] C. E. Demirci Dönmez, P. K. Manna, R. Nickel, S. Aktürk, and J. van Lierop, Comparative heating efficiency of cobalt-, manganese-, and nickel-ferrite nanoparticles for a hyperthermia agent in biomedicines, *ACS Appl. Mater. Interfaces* **11**, 6858 (2019).
- [3] P. B. Balakrishnan, N. Silvestri, T. Fernandez-Cabada, F. Marinaro, S. Fernandes, S. Fiorito, M. Miscuglio, D. Serantes, S. Ruta, K. Livesey *et al.*, Exploiting unique alignment of cobalt ferrite nanoparticles, mild hyperthermia, and controlled intrinsic cobalt toxicity for cancer therapy, *Adv. Mater.* **32**, 2003712 (2020).
- [4] S. K. Dutta, M. Akhter, J. Ahmed, M. K. Amin, and P. K. Dhar, Synthesis and catalytic activity of spinel ferrites: A brief review, *Biointerface Res. Appl. Chem.* **12**, 4399 (2021).
- [5] S. K. Paswan, P. Kumar, R. K. Singh, S. K. Shukla, and L. Kumar, Spinel ferrite magnetic nanoparticles, in *Pollutants and Water Management* (John Wiley & Sons, Hoboken, NJ, 2021) Chap. 11, p. 273
- [6] H. Hajiyani and R. Pentcheva, Surface termination and composition control of activity of the $\text{Co}_x\text{Ni}_{1-x}\text{Fe}_2\text{O}_4(001)$ surface for water oxidation: Insights from DFT + U calculations, *ACS Catal.* **8**, 11773 (2018).
- [7] B. I. Kharisov, H. R. Dias, and O. V. Kharissova, Mini-review: Ferrite nanoparticles in the catalysis, *Arab. J. Chem.* **12**, 1234 (2019).
- [8] M. Bohra, V. Alman, and R. Arras, Nanostructured ZnFe_2O_4 : An exotic energy material, *Nanomaterials* **11**, 1286 (2021).
- [9] D. H. Taffa, R. Dillert, A. C. Ulpe, K. C. L. Bauerfeind, T. Bredow, D. W. Bahnemann, and M. Wark, Photoelectrochemical and theoretical investigations of spinel type ferrites ($M_x\text{Fe}_{3-x}\text{O}_4$) for water splitting: A mini-review, *J. Photon. Energy* **7**, 012009 (2016).
- [10] R. Valenzuela, Novel applications of ferrites, *Phys. Res. Int.* **2012**, 591839 (2012).
- [11] A. Hirohata, H. Sukegawa, H. Yanagihara, I. Žutić, T. Seki, S. Mizukami, and R. Swaminathan, Roadmap for emerging materials for spintronic device applications, *IEEE Trans. Magn.* **51**, 1 (2015).
- [12] A. Yanase and K. Siratori, Band structure in the high temperature phase of Fe_3O_4 , *J. Phys. Soc. Jpn.* **53**, 312 (1984).

- [13] J.-B. Moussy, From epitaxial growth of ferrite thin films to spin-polarized tunnelling, *J. Phys. D: Appl. Phys.* **46**, 143001 (2013).
- [14] C. A. F. Vaz, J. Hoffman, C. H. Ahn, and R. Ramesh, Magnetoelectric coupling effects in multiferroic complex oxide composite structures, *Adv. Mater.* **22**, 2900 (2010).
- [15] X. Yang, Z. Zhou, T. Nan, Y. Gao, G. M. Yang, M. Liu, and N. X. Sun, Recent advances in multiferroic oxide heterostructures and devices, *J. Mater. Chem. C* **4**, 234 (2016).
- [16] C. Song, B. Cui, F. Li, X. Zhou, and F. Pan, Recent progress in voltage control of magnetism: Materials, mechanisms, and performance, *Prog. Mater. Sci.* **87**, 33 (2017).
- [17] W. Hu, N. Qin, G. Wu, Y. Lin, S. Li, and D. Bao, Opportunity of spinel ferrite materials in nonvolatile memory device applications based on their resistive switching performances, *J. Am. Chem. Soc.* **134**, 14658 (2012).
- [18] X. Chen, X. Zhu, W. Xiao, G. Liu, Y. P. Feng, J. Ding, and R.-W. Li, Nanoscale magnetization reversal caused by electric field-induced ion migration and redistribution in cobalt ferrite thin films, *ACS Nano* **9**, 4210 (2015).
- [19] P. Dhanapal, S. Guo, B. Wang, H. Yang, S. Agarwal, Q. Zhan, and R.-W. Li, High-throughput Investigation of Orientations Effect on Nanoscale Magnetization Reversal in Cobalt Ferrite thin Films Induced by Electric Field, *Appl. Phys. Lett.* **111**, 162401 (2017).
- [20] S. Munjal and N. Khare, Valence change bipolar resistive switching accompanied with magnetization switching in CoFe_2O_4 thin film, *Sci. Rep.* **7**, 12427 (2017).
- [21] S. Robbenolt, E. Menéndez, A. Quintana, A. Gómez, S. Auffret, V. Baltz, E. Pellicer, and J. Sort, Reversible, electric-field induced magneto-ionic control of magnetism in mesoporous cobalt ferrite thin films, *Sci. Rep.* **9**, 10804 (2019).
- [22] J. K. Burdett, G. D. Price, and S. L. Price, Role of the crystal-field theory in determining the structures of spinels, *J. Am. Chem. Soc.* **104**, 92 (1982).
- [23] K. R. Sanchez-Lievano, J. L. Stair, and K. E. Knowles, Cation distribution in spinel ferrite nanocrystals: Characterization, impact on their physical properties, and opportunities for synthetic control, *Inorg. Chem.* **60**, 4291 (2021).
- [24] A. V. Ramos, T. S. Santos, G. X. Miao, M.-J. Guittet, J.-B. Moussy, and J. S. Moodera, Influence of oxidation on the spin-filtering properties of CoFe_2O_4 and the resultant spin polarization, *Phys. Rev. B* **78**, 180402(R) (2008).
- [25] J. A. Moyer, C. A. F. Vaz, E. Negusse, D. A. Arena, and V. E. Henrich, Controlling the electronic structure of $\text{Co}_{1-x}\text{Fe}_{2+x}\text{O}_4$ thin films through iron doping, *Phys. Rev. B* **83**, 035121 (2011).
- [26] R. Arras, L. Calmels, and B. Warot-Fonrose, Half-Metallicity, Magnetic Moments, and Gap States in Oxygen-Deficient Magnetite for Spintronic Applications, *Appl. Phys. Lett.* **100**, 032403 (2012).
- [27] R. Arras, B. Warot-Fonrose, and L. Calmels, Electronic structure near cationic defects in magnetite, *J. Phys.: Condens. Matter* **25**, 256002 (2013).
- [28] K. Dileep, B. Loukya, N. Pachauri, A. Gupta, and R. Datta, Probing optical band gaps at the nanoscale in NiFe_2O_4 and CoFe_2O_4 epitaxial films by high resolution electron energy loss spectroscopy, *J. Appl. Phys.* **116**, 103505 (2014).
- [29] Y. H. Hou, Y. J. Zhao, Z. W. Liu, H. Y. Yu, X. C. Zhong, W. Q. Qiu, D. C. Zeng, and L. S. Wen, Structural, electronic and magnetic properties of partially inverse spinel CoFe_2O_4 : A first-principles study, *J. Phys. D: Appl. Phys.* **43**, 445003 (2010).
- [30] D. Fritsch and C. Ederer, Effect of epitaxial strain on the cation distribution in spinel ferrites CoFe_2O_4 and NiFe_2O_4 : A Density Functional Theory Study, *Appl. Phys. Lett.* **99**, 081916 (2011).
- [31] D. Fritsch and C. Ederer, First-principles calculation of magnetoelastic coefficients and magnetostriction in the spinel ferrites CoFe_2O_4 and NiFe_2O_4 , *Phys. Rev. B* **86**, 014406 (2012).
- [32] D. Odkhuu, P. Taivansaikhan, W. S. Yun, and S. C. Hong, A first-principles study of magnetostrictions of Fe_3O_4 and CoFe_2O_4 , *J. Appl. Phys.* **115**, 17A916 (2014).
- [33] C. L. Muhich, V. J. Aston, R. M. Trotter, A. W. Weimer, and C. B. Musgrave, First-principles analysis of cation diffusion in mixed metal ferrite spinels, *Chem. Mater.* **28**, 214 (2016).
- [34] G. Kresse and J. Hafner, Ab initio molecular-dynamics simulation of the liquid-metal-amorphous-semiconductor transition in germanium, *Phys. Rev. B* **49**, 14251 (1994).
- [35] G. Kresse and J. Furthmüller, Efficient iterative schemes for *ab initio* total-energy calculations using a plane-wave basis set, *Phys. Rev. B* **54**, 11169 (1996).
- [36] P. E. Blöchl, Projector augmented-wave method, *Phys. Rev. B* **50**, 17953 (1994).
- [37] J. P. Perdew, A. Ruzsinszky, G. I. Csonka, O. A. Vydrov, G. E. Scuseria, L. A. Constantin, X. Zhou, and K. Burke, Restoring the Density-Gradient Expansion for Exchange in Solids and Surfaces, *Phys. Rev. Lett.* **100**, 136406 (2008); **102**, 039902(E) (2009).
- [38] S. L. Dudarev, G. A. Botton, S. Y. Savrasov, C. J. Humphreys, and A. P. Sutton, Electron-energy-loss spectra and the structural stability of nickel oxide: An LSDA + U study, *Phys. Rev. B* **57**, 1505 (1998).
- [39] V. N. Antonov, B. N. Harmon, and A. N. Yaresko, Electronic structure and x-ray magnetic circular dichroism in Fe_3O_4 and Mn-, Co-, or Ni-substituted Fe_3O_4 , *Phys. Rev. B* **67**, 024417 (2003).
- [40] Q. C. Sun, H. Sims, D. Mazumdar, J. X. Ma, B. S. Holinsworth, K. R. O'Neal, G. Kim, W. H. Butler, A. Gupta, and J. L. Musfeldt, Optical band gap hierarchy in a magnetic oxide: Electronic structure of NiFe_2O_4 , *Phys. Rev. B* **86**, 205106 (2012).
- [41] B. S. Holinsworth, D. Mazumdar, H. Sims, Q.-C. Sun, M. K. Yurtisigi, S. K. Sarker, A. Gupta, W. H. Butler, and J. L. Musfeldt, Chemical tuning of the optical band gap in spinel ferrites: CoFe_2O_4 vs NiFe_2O_4 , *Appl. Phys. Lett.* **103**, 082406 (2013).
- [42] H. J. Monkhorst and J. D. Pack, Special points for Brillouin-zone integrations, *Phys. Rev. B* **13**, 5188 (1976).
- [43] See Supplemental Material at <http://link.aps.org/supplemental/10.1103/PhysRevMaterials.6.124402> for a description of the atomic structures. Details on the calculations to obtain the inversion degrees as a function of the temperature, to calculate the magnetic properties and the thermodynamic phase diagrams are also provided.
- [44] H. T. Stokes and D. M. Hatch, *FINDSYM*: program for identifying the space-group symmetry of a crystal, *J. Appl.*

- Crystallogr.* **38**, 237 (2005); H. T. Stokes, D. M. Hatch, and B. J. Campbell, ISOTROPY Software Suite, iso.byu.edu.
- [45] M. I. Aroyo, A. Kirov, C. Capillas, J. M. Perez-Mato, and H. Wondratschek, Bilbao Crystallographic Server. II. Representations of crystallographic point groups and space groups, *Acta Crystallogr. Sect. A* **62**, 115 (2006).
- [46] A. M. Iliia, P.-M. J. Manuel, C. Cesar, K. Eli, I. Svetoslav, M. Gotzon, K. Asen, and W. Hans, Bilbao Crystallographic Server: I. Databases and crystallographic computing programs, *Z. Kristallogr. - Cryst. Mater.* **221**, 15 (2009).
- [47] R. Grau-Crespo, S. Hamad, C. R. A. Catlow, and N. H. de Leeuw, Symmetry-adapted configurational modelling of fractional site occupancy in solids, *J. Phys.: Condens. Matter* **19**, 256201 (2007).
- [48] C. Freysoldt, B. Grabowski, T. Hickel, J. Neugebauer, G. Kresse, A. Janotti, and C. G. Van de Walle, First-principles calculations for point defects in solids, *Rev. Mod. Phys.* **86**, 253 (2014).
- [49] E. Péan, J. Vidal, S. Jobic, and C. Latouche, Presentation of the PyDEF Post-Treatment Python Software to Compute Publishable Charts for Defect Energy Formation, *Chem. Phys. Lett.* **671**, 124 (2017).
- [50] S. Kim, S. N. Hood, J.-S. Park, L. D. Whalley, and A. Walsh, Quick-start guide for first-principles modelling of point defects in crystalline materials, *J. Phys. Energy* **2**, 036001 (2020).
- [51] S. Lany and A. Zunger, Accurate prediction of defect properties in density functional supercell calculations, *Model. Simul. Mater. Sci. Eng.* **17**, 084002 (2009).
- [52] G. Makov and M. C. Payne, Periodic boundary conditions in *ab initio* calculations, *Phys. Rev. B* **51**, 4014 (1995).
- [53] A. Stoliaroff, S. Jobic, and C. Latouche, PyDEF 2.0: An easy to use post-treatment software for publishable charts featuring a graphical user interface, *J. Comput. Chem.* **39**, 2251 (2018).
- [54] D. Gutiérrez, M. Foerster, I. Fina, J. Fontcuberta, D. Fritsch, and C. Ederer, Dielectric response of epitaxially strained CoFe_2O_4 spinel thin films, *Phys. Rev. B* **86**, 125309 (2012).
- [55] V. Kosyak, N. B. Mortazavi Amiri, A. V. Postnikov, and M. A. Scarpulla, Model of native point defect equilibrium in $\text{Cu}_2\text{ZnSnS}_4$ and application to one-zone annealing, *J. Appl. Phys.* **114**, 124501 (2013).
- [56] G. Geneste, C. Paillard, and B. Dkhil, Polarons, vacancies, vacancy associations, and defect states in multiferroic BiFeO_3 , *Phys. Rev. B* **99**, 024104 (2019).
- [57] D. Krasikov, A. Knizhnik, B. Potapkin, and T. Sommerer, Why shallow defect levels alone do not cause high resistivity in *cdte*, *Semicond. Sci. Technol.* **28**, 125019 (2013).
- [58] T. Aghavonian, J.-B. Moussy, D. Stanescu, R. Belkhou, N. Jedrecy, H. Magnan, P. Ohresser, M.-A. Arrio, P. Saintavit, and A. Barbier, Determination of the cation site distribution of the spinel in multiferroic $\text{CoFe}_2\text{O}_4/\text{BaTiO}_3$ layers by x-ray photoelectron spectroscopy, *J. Electron Spectrosc. Relat. Phenom.* **202**, 16 (2015).
- [59] E. Martin, F. Roulland, S. Grenier, F. Appert, J. Juraszek, M. Trassin, C. Bouillet, E. Chikoidze, C. Arnold, B. Berini *et al.*, Non-auxetic/auxetic transitions inducing modifications of the magnetic anisotropy in CoFe_2O_4 thin films, *J. Alloys Compd.* **836**, 155425 (2020).
- [60] R. Arras and L. Calmels, Fully spin-polarized two-dimensional electron gas at the $\text{CoFe}_2\text{O}_4/\text{MgAl}_2\text{O}_4(001)$ polar interface, *Phys. Rev. B* **90**, 045411 (2014).
- [61] P. V. Balachandran and J. M. Rondinelli, Massive band gap variation in layered oxides through cation ordering, *Nat. Commun.* **6**, 6191 (2015).
- [62] J. Young, E. J. Moon, D. Mukherjee, G. Stone, V. Gopalan, N. Alem, S. J. May, and J. M. Rondinelli, Polar oxides without inversion symmetry through vacancy and chemical order, *J. Am. Chem. Soc.* **139**, 2833 (2017).
- [63] E. J. W. Verwey and E. L. Heilmann, Physical properties and cation arrangement of oxides with spinel structures I. Cation arrangement in spinels, *J. Chem. Phys.* **15**, 174 (1947).
- [64] E. J. Verwey, P. W. Haayman, and F. C. Romeijn, Physical properties and cation arrangement of oxides with spinel structures II. Electronic conductivity, *J. Chem. Phys.* **15**, 181 (1947).
- [65] E. J. W. Verwey, F. de Boer, and J. H. van Santen, Cation arrangement in spinels, *J. Chem. Phys.* **16**, 1091 (1948).
- [66] P. W. Anderson, Ordering and antiferromagnetism in ferrites, *Phys. Rev.* **102**, 1008 (1956).
- [67] A. Miller, Distribution of cations in spinels, *J. Appl. Phys.* **30**, S24 (1959).
- [68] C. Haas, Phase transitions in crystals with the spinel structure, *J. Phys. Chem. Solids* **26**, 1225 (1965).
- [69] D. Sharma and N. Khare, Tuning of optical bandgap and magnetization of CoFe_2O_4 thin films, *Appl. Phys. Lett.* **105**, 032404 (2014).
- [70] V. G. Ivanov, M. V. Abrashev, M. N. Iliev, M. M. Gospodinov, J. Meen, and M. I. Aroyo, Short-range *b*-site ordering in the inverse spinel ferrite NiFe_2O_4 , *Phys. Rev. B* **82**, 024104 (2010).
- [71] J. K. Dey, A. Chatterjee, S. Majumdar, A.-C. Dippel, O. Gutowski, M. v. Zimmermann, and S. Giri, Ferroelectric order associated with ordered occupancy at the octahedral site of the inverse spinel structure of multiferroic NiFe_2O_4 , *Phys. Rev. B* **99**, 144412 (2019).
- [72] H.-T. Jeng, G. Y. Guo, and D. J. Huang, Charge-orbital ordering in low-temperature structures of magnetite: GGA + *U* investigations, *Phys. Rev. B* **74**, 195115 (2006).
- [73] V. Stevanović, M. d'Avezac, and A. Zunger, Universal electrostatic origin of cation ordering in A_2BO_4 spinel oxides, *J. Am. Chem. Soc.* **133**, 11649 (2011).
- [74] J. Liu, X. Wang, O. J. Borkiewicz, E. Hu, R.-J. Xiao, L. Chen, and K. Page, Unified view of the local cation-ordered state in inverse spinel oxides, *Inorg. Chem.* **58**, 14389 (2019).
- [75] Z. Li, J. Lu, L. Jin, J. Rusz, V. Kocovski, H. Yanagihara, E. Kita, J. Mayer, R. E. Dunin-Borkowski, H. Xiang *et al.*, Atomic structure and electron magnetic circular dichroism of individual rock salt structure antiphase boundaries in spinel ferrites, *Adv. Funct. Mater.* **31**, 2008306 (2021).
- [76] U.-G. Jong, C.-J. Yu, Y.-S. Park, and C.-S. Ri, First-principles study of ferroelectricity induced by p-d hybridization in ferromagnetic NiFe_2O_4 , *Phys. Lett. A* **380**, 3302 (2016).
- [77] R. C. Liebermann, Pressure and temperature dependence of the elastic properties of polycrystalline trevorite (NiFe_2O_4), *Phys. Earth Planet. Inter.* **6**, 360 (1972).
- [78] Z. Li, E. S. Fisher, J. Z. Liu, and M. V. Nevitt, Single-crystal elastic constants of Co-Al and Co-Fe spinels, *J. Mater. Sci.* **26**, 2621 (1991).

- [79] A. C. Ulpe, K. C. L. Bauerfeind, and T. Bredow, Influence of spin state and cation distribution on stability and electronic properties of ternary transition-metal oxides, *ACS Omega* **4**, 4138 (2019).
- [80] M. Meinert and G. Reiss, Electronic structure and optical band gap determination of NiFe_2O_4 , *J. Phys.: Condens. Matter* **26**, 115503 (2014).
- [81] Z. Szotek, W. M. Temmerman, D. Ködderitzsch, A. Svane, L. Petit, and H. Winter, Electronic structures of normal and inverse spinel ferrites from first principles, *Phys. Rev. B* **74**, 174431 (2006).
- [82] A. Walsh, S.-H. Wei, Y. Yan, M. M. Al-Jassim, J. A. Turner, M. Woodhouse, and B. A. Parkinson, Structural, magnetic, and electronic properties of the Co-Fe-Al oxide spinel system: Density-functional theory calculations, *Phys. Rev. B* **76**, 165119 (2007).
- [83] S. Sharifi, A. Yazdani, and K. Rahimi, Incremental substitution of Ni with Mn in NiFe_2O_4 to largely enhance its supercapacitance properties, *Sci. Rep.* **10**, 10916 (2020).
- [84] M. Pénicaud, B. Siberchicot, C. B. Sommers, and J. Kübler, Calculated electronic band structure and magnetic moments of ferrites, *J. Magn. Magn. Mater.* **103**, 212 (1992).
- [85] V. Stevanović, M. d’Avezac, and A. Zunger, Simple Point-Ion Electrostatic Model Explains the Cation Distribution in Spinel Oxides, *Phys. Rev. Lett.* **105**, 075501 (2010).
- [86] H. S. C. O’Neill and A. Navrotsky, Simple spinels; crystallographic parameters, cation radii, lattice energies, and cation distribution, *Am. Mineral.* **68**, 181 (1983).
- [87] Y. Seminovski, P. Palacios, P. Wahnón, and R. Grau-Crespo, Band gap control via tuning of inversion degree in CdIn_2S_4 spinel, *Appl. Phys. Lett.* **100**, 102112 (2012).
- [88] D. Santos-Carballal, A. Roldan, R. Grau-Crespo, and N. H. de Leeuw, First-principles study of the inversion thermodynamics and electronic structure of FeM_2X_4 (thio)spinel ($M = \text{Cr}, \text{Mn}, \text{Co}, \text{Ni}$; $X = \text{O}, \text{S}$), *Phys. Rev. B* **91**, 195106 (2015).
- [89] M. N. Iliev, D. Mazumdar, J. X. Ma, A. Gupta, F. Rigato, and J. Fontcuberta, Monitoring *B*-site ordering and strain relaxation in NiFe_2O_4 epitaxial films by polarized Raman spectroscopy, *Phys. Rev. B* **83**, 014108 (2011).
- [90] D. Carta, M. F. Casula, A. Falqui, D. Loche, G. Mountjoy, C. Sangregorio, and A. Corrias, A structural and magnetic investigation of the inversion degree in ferrite nanocrystals MFe_2O_4 ($M = \text{Mn}, \text{Co}, \text{Ni}$), *J. Phys. Chem. C* **113**, 8606 (2009).
- [91] G. A. Sawatzky, F. Van Der Woude, and A. H. Morrish, Mössbauer study of several ferrimagnetic spinels, *Phys. Rev.* **187**, 747 (1969).
- [92] N. Jedrecy, T. Aghavonian, J.-B. Moussy, H. Magnan, D. Stanesco, X. Portier, M.-A. Arrio, C. Mocuta, A. Vlad, R. Belkhou *et al.*, Cross-correlation between strain, ferroelectricity, and ferromagnetism in epitaxial multiferroic $\text{CoFe}_2\text{O}_4/\text{BaTiO}_3$ heterostructures, *ACS Appl. Mater. Interfaces* **10**, 28003 (2018).
- [93] R. Safi, A. Ghasemi, R. Shoja-Razavi, and M. Tavousi, The role of pH on the particle size and magnetic consequence of cobalt ferrite, *J. Magn. Magn. Mater.* **396**, 288 (2015).
- [94] S. Hunpraturub, S. Phokha, P. Kidkhunthod, N. Chanlek, and P. Chindaprasirt, The effect of cation distribution on the magnetic properties of CoFe_2O_4 nanoparticles, *Results Phys.* **24**, 104112 (2021).
- [95] C. Moya, A. Fraile Rodríguez, M. Escoda-Torroella, M. García del Muro, S. R. V. Avula, C. Piamonteze, X. Batlle, and A. Labarta, Crucial role of the Co cations on the destabilization of the ferrimagnetic alignment in Co-ferrite nanoparticles with tunable structural defects, *J. Phys. Chem. C* **125**, 691 (2021).
- [96] R. Grau-Crespo, A. Y. Al-Baitai, I. Saadoun, and N. H. D. Leeuw, Vacancy ordering and electronic structure of $\gamma\text{-Fe}_2\text{O}_3$ (maghemite): A theoretical investigation, *J. Phys.: Condens. Matter* **22**, 255401 (2010).
- [97] X. Shi, Y.-F. Li, S. L. Bernasek, and A. Selloni, Structure of the $\text{NiFe}_2\text{O}_4(001)$ surface in contact with gaseous O_2 and water vapor, *Surf. Sci.* **640**, 73 (2015), reactivity concepts at surfaces: Coupling theory with experiment.
- [98] V. Stevanović, S. Lany, X. Zhang, and A. Zunger, Correcting density functional theory for accurate predictions of compound enthalpies of formation: Fitted elemental-phase reference energies, *Phys. Rev. B* **85**, 115104 (2012).
- [99] Z. Rák, C. O’Brien, and D. Brenner, First-principles investigation of boron defects in nickel ferrite spinel, *J. Nucl. Mater.* **452**, 446 (2014).
- [100] J. Osorio-Guillén, S. Lany, S. V. Barabash, and A. Zunger, Magnetism without Magnetic Ions: Percolation, Exchange, and Formation Energies of Magnetism-Promoting Intrinsic Defects in CaO, *Phys. Rev. Lett.* **96**, 107203 (2006).
- [101] K. Reuter and M. Scheffler, Composition, structure, and stability of $\text{RuO}_2(110)$ as a function of oxygen pressure, *Phys. Rev. B* **65**, 035406 (2001).
- [102] R. C. Weast and M. J. Astle, eds., *CRC Handbook of Chemistry and Physics* (CRC Press, Boca Raton, 1979).
- [103] G. H. Jaffari, A. K. Rumaiz, J. C. Woicik, and S. I. Shah, Influence of oxygen vacancies on the electronic structure and magnetic properties of NiFe_2O_4 thin films, *J. Appl. Phys.* **111**, 093906 (2012).